



Stockholm
University

Master Thesis

Degree Project in
Geology 45 hp

Reconstructing Paleoclimate Changes in Northern Store Mosse: Minerals, Organic Matter and Climate

Jenny Gåling



Stockholm 2019

Department of Geological Sciences
Stockholm University
SE-106 91 Stockholm

Reconstructing Paleoclimate Changes in northern Store Mosse:
Minerals, Organic Matter and Climate

Front page: View over Store Mosse, “The Great Bog” with sand dune ridge in the distance.
Photo: Malin Kylander, 2018

Abstract

Ombrotrophic peat bogs only receive minerogenic material from atmospheric deposition and thus, they are excellent archives of aeolian derived dust, which can act as an important climate factor. Here, 4800 years of paleoclimatic change was reconstructed from a peat core collected from northern Store Mosse, southern Sweden (57°16'37.70"N, 13°55'30.86"E). The site is located only one kilometre south of an extensive sand dune system that bisects the north-eastern peatland. Previous work by Kylander et al. (2018) implies a shift in the mineral dust source between 5500 and 4500 years ago to less weathered, more coarse-grained, P-rich minerals and feldspars. The provenance of this dust source is yet unknown, but a local source is hypothesised. The basis of this thesis is to conceive if the dust signal is more pronounced in the northern Store Mosse, neighbouring the sand dune ridge.

Calculation of bulk density along with age-depth modelling of radiocarbon dates enabled net PAR to be determined. Through ATR-FTIR analyses of bulk and ashed peat samples, different organic and inorganic compounds of the peat could be identified. This was facilitated using a principal component analysis of the two datasets separately. Additionally, XRF-CS analyses of discrete ashed peat samples were performed and elements were clustered using principal component analysis. The bulk density and PAR values indicate an initial fen stage, and after the fen-bog transition around 4200 cal yr BP follows major shifts at 3500, 2100, 890 and 660 cal yr BP which are interpreted as at least three successive bog stages. These changes are coupled to variation in the factor scores for spectral components explaining the gradual decomposition, mobile elements, bog vegetation changes and relative amounts of important organic compounds of peat (polysaccharides, hydrocarbons, acids and lipids). The spectral data further indicate the source shifts for the aeolian dust and fluctuations in the deposition of quartz and feldspar minerals throughout the peat core. The changes in minerals was coupled to the elemental data and show a shift in mineral influx during the last 2500 years, with ten significant increases of more coarse-grained material. These short periods occur during periods of increased storminess in northern Europe, dated to 1900-1050 and 600-250 cal yr BP. Conclusively, spectral and elemental data of inorganic peat from the northern Store Mosse show a potential storm-signal.

Sammanfattning

Ombrotrofa torvmossor får endast minerogent material från atmosfäriskt nedfall och är således utmärkta arkiv för stoft av eoliskt ursprung, vilket kan påverka klimatet. I detta arbete har 4800 år av paleoklimatologiska variationer rekonstruerats från en torvkärna som insamlats från norra Store Mosse i södra Sverige (57°16'37.70"N, 13°55'30.86"Ö). Platsen ligger endast en kilometer söder om ett omfattande sanddynssystem, vilket korsar den nordvästra delen av myren. Tidigare studier av Kylander et al. (2018) har visat att det eoliska stoftet har ett annat ursprung omkring 5500–4500 cal B.P., med nedfall av mindre vittrade, grovkorniga och fosfat-rika mineral och fältspater. Härkomsten av detta minerogena material är ännu okänd, men det har resonerats om ett lokalt ursprung. Grunden till detta arbete ligger i att utröna huruvida det eoliska dammet har en tydligare signal närmare sanddynerna i den norra delen av Store Mosse.

Beräkningar av bulkdensitet och åldersmodellering av kol-14 dateringar möjliggjorde vidare att beräkningar av ackumulationshastighet kunde göras för hela torvsekvensen. Genom att analysera bulk- och askade torvprover kunde olika organiska och oorganiska komponenter identifieras. Detta förenklades med separata principalkomponentanalyser för de två dataseten. Vidare analyserades de enskilda askade proverna med röntgenfluorescens (XRF-CS) och resultatet grupperades även då med principalkomponentanalys. Resultatet från analyser av bulkdensitet och ackumulationshastighet över tid visar ett inledande kärr stadium som skiftar till mosse omkring 4200 cal B.P. Tydliga förändringar kunde därefter ses omkring 3500, 2100, 890 och 660 cal B.P., vilket indikerar minst tre på varandra efterföljande mosse stadier. Dessa variationer har kopplats till spektrografiska data, och förändringar i faktornvärdena för de faktorer som förklarar gradvis nedbrytning, mobila ämnen, vegetation samt viktiga organiska beståndsdelar i torv (polysackarider, kolväten, syror och lipider). En tydlig förändring av ursprunget för det eoliska dammet samt omväxlande kvarts och fältspater har observerats genom hela torvsekvensen. Vidare har dessa variationer av mineral kopplats till grundämnesdata, vilket visar på ett ökat inflöde av mer grovkornigt material vid tio korta perioder sedan 2500 cal B.P. Dessa perioder inträffar under en längre tid av ökad frekvens och intensitet av stormar i norra Europa omkring 1900–1050 samt 600–250 cal B.P. Sammanfattningsvis så har detta tolkats som en potentiell storm signal i den minerogena delen av torvsekvensen från norra Store Mosse.

Table of contents

1	Introduction.....	6
1.1	Project Aims	6
2	Background.....	7
2.1	Peatland Development.....	7
2.2	Atmospheric Dust	8
2.3	Methods for the Characterization of Peat and Peat Ash	9
2.4	Radiocarbon Dating	10
2.5	Late-Holocene Climate Variability.....	10
3	Study Area	11
3.1	Site Description	11
3.2	The Store Mosse Bog During the Holocene.....	13
3.3	Climate and Storminess Affecting Store Mosse	13
4	Analytical Materials and Methods.....	14
4.1	Sampling.....	14
4.2	Analyses.....	14
4.3	Statistical Analyses.....	16
5	Results	17
5.1	Store Mosse Dune South (SMDS) Age-depth Modelling.....	17
5.2	Organic Bulk Density, Ash Content and PAR.....	18
5.3	Principal Component Analysis on ATR-FTIR Data	18
5.4	Elemental Data from X-ray Fluorescence Core Scanning (XRF-CS)	24
6	Discussion.....	25
6.1	Peatland Development.....	25
6.2	Spectral Signals from the Bulk Peat.....	27
6.3	Spectral Signals from the Ashed Peat	29
6.4	Interpretation of Changes in Spectral Data Over Time	30
6.5	Interpretation of Elemental Data.....	31
6.6	Paleoclimatic Summary	32
7	Conclusions and Future Prospects	37
8	Acknowledgements.....	37
9	References	38
10	Appendix.....	41
10.1	Photos of the Fresh SMDS Core Sections	41
10.2	Specifications for the ATR device.....	41
10.3	Freeze-drier and Pump	41
10.4	Age-depth Model.....	42
10.5	Selection of Absorption Peaks	43
10.6	XRF-CS Elemental Data Profiles	45
10.7	Interpretation of ATF-FTIR Wavenumbers	46

1 Introduction

Previous paleoclimate research at Store Mosse, “the Great Bog”, in southern Sweden has been focused mainly in the southern part of the bog. These deposits in the southern bog have been used in paleoclimate reconstructions looking at changes in effective humidity, mineral dust, nutrient input, vegetation changes and bog development (Kylander et al., 2013, 2016, 2018; Malmer et al., 1997; Svensson, 1988a). Results from these records show a notably high peat accumulation event around 4500-5500 years ago in the southern part of Store Mosse. Available geochemical data from this site shows that there is also a significant shift in the mineral dust composition during this time, with deposition of less weathered, more coarse-grained, P-rich minerals and feldspars (Kylander et al., 2016). The source of this material is yet unknown, but it is suggested that a local source has been activated during increased storminess from the climate shifts occurring at the time. It is hypothesised that a suitable local source is the sand dune system that formed before peat accumulation began in Store Mosse and bisects the peatland today. Previous work by Kylander et al. (2018) has been conducted at sampling sites located 4-6.5 km from the sand dunes. If the sand dunes in the area were activated during the mid-Holocene, as suggested above, an increased mineral dust signal is expected closer to the dunes. The basis for this thesis is a core collected around one kilometre south of this dune system, Store Mosse Dune South (SMDS).

Fourier Transform Infrared (FTIR) spectroscopy can be used to analyse geological samples and for identification of important components therein (such as lignin, polysaccharides, aromatics, minerals, etc.). If this information is processed statistically, one can see how mineral matter and vegetation dynamics have varied in the past and how they are linked to climate changes (e.g. precipitation, temperature). Also, FTIR has several advantages which includes fast analysis time, need of very little sample material and easy acquisition of large amounts of data.

1.1 Project Aims

The thesis consists of both an analytical development component as well as a climate reconstruction component. The aim of the thesis is to fulfil the following objectives in the previously understudied northern sections of Store Mosse:

1. Perform FTIR spectroscopy on bulk peat and ashed peat samples and discuss differences between the two.
2. Identify major deposit transitions (fen-bog boundary) and significant shifts in decomposition using bulk density data.
3. Age date the basal proportion of the extended sequence and calculate peat accumulation rates (PAR) based on bulk density and ^{14}C data.
4. Discuss how the inorganic and organic components of the peat have changed over time and what these changes say about past climate changes (effective humidity, mineral dust deposition and storminess).
5. Reconstruct past climate changes focusing on effective humidity, mineral dust deposition and storminess.
6. Compare the paleoclimate records from the northern SMDS with previous southern records of Store Mosse.

2 Background

Peatland environmental research gives us information about the surroundings of the peat and the organic and inorganic compounds of peat, where the hydrology and ecology of the peatland itself are central aspects for the internal peatland environment. The peatland, or mire, is best understood through studying as many aspects of the peat as possible, including external forcing factors (Charman, 2002).

2.1 Peatland Development

Peat accumulation occur where primary productivity exceeds ecosystem respiration and is formed from partial decomposition of plant litter. The peatland ecosystems have had a larger net primary production than decomposition and as a result, peat has formed from carbon-rich (40-50%) organic matter that has accumulated over time (Wieder & Vitt, 2006). Peatlands are an important constituent of the global carbon pool and are estimated to store around 1400×10^9 tonnes C, which equals a third to a half of the global soil carbon pool. This means that there is almost as much carbon in peat as is present in the entire global atmospheric carbon pool (Charman, 2002). Peatlands occupy around 4×10^6 km² globally, where boreal peatlands account for 86% of these. Peatlands occur mainly in areas with cold-temperate boreal climate, in many previously glaciated regions (Kylander et al., 2018; Wieder & Vitt, 2006). Around 15% of Sweden's area consists of peatlands.

Peatlands form either from a shallow lake (terrestrialisation), a process which does not require environmental change, or on mineral soil (paludification) (Charman, 2002). Terrestrialisation occur when soils are saturated seasonally or all year and are influenced and recharged with nutrient-rich waters from surrounding soils, and these conditions allow varying degrees of organic matter accumulation (Wieder & Vitt, 2006). Accumulated debris gradually fills the shallow water, initiating fen peat formation that may be replaced by bog peat formation in a later stage.

The net PAR in peatlands can vary greatly over time and is determined by several factors including nutrient availability, deposit hydrology and surface vegetation (Kylander et al., 2018). Simplified, PAR is determined by production and decay rates, where the latter is most important. Both of these processes mainly occur in the acrotelm, the aerobic and active layer of the peat column. The catotelm is everything below the surface layer, where decay rates are significantly slower due to anoxic and waterlogged conditions (Charman, 2002). Mineralisation of peat into carbon dioxide and water is also faster under aerobic than anaerobic conditions (Wieder & Vitt, 2006).

Another fundamental aspect for describing peatlands is the nutrient status, which range from relatively nutrient-rich conditions (fen; Sv. *mosse*) towards very poor conditions (bog; Sv. *kärr*) (Charman, 2002). Fens are influenced by ground or surface water and thus larger nutrient input, while bogs are mineral-poor and ombrotrophic which implies a nutrient supply only from water in atmospheric deposition falling onto its surface (Charman, 2002; Loisel et al., 2014). Because of their ombrotrophic nature, bogs are excellent climate archives. Bogs commonly develop from fens, and the raised bog stratigraphy usually show the fen-bog transition (Charman, 2002). Either vertical peat accumulation or a lowered water table will result in disconnection from water supply from below, which leads to ombrotrophic conditions (Hughes & Barber, 2003). Nutrient poor conditions from vertical peat accumulation is promoted by a small amount of degradation and *Sphagnum* growth during a period of wet climate (high precipitation), generating a small amount of degradation that is beneficial for *Sphagnum* growth (Hughes & Barber, 2003). The alternative is lowering of the

groundwater table, which causes decreased bog surface wetness and increased aerobic conditions and decomposition (Hughes & Barber, 2003).

The degree of peat decay or humification is used to reconstruct a surface wetness record of an ombrotrophic peatland (Charman, 2002). The degree of humification (DOH) can be measured via a proxy called (organic) bulk density. More fine-grained peat is more decomposed, and more fine-grained material should yield higher bulk density values (Björck & Clemmensen, 2004). There is growing evidence that changes in surface wetness in ombrotrophic peatlands can be strongly related to either temperature or precipitation, but it is still not clear which of the two climatic parameters that is more important, and it may vary globally. Generally, there is a systematic relationship between peat depth and humification, due to the continuous decay of peat over time. A high DOH implies dry and warm conditions, while low DOH implies reduced decay and wet and cool conditions (Charman, 2002). These variations in DOH and bulk density are often used in ombrotrophic mires to reconstruct climatic changes.

Sphagnum peat is dominated by *Sphagnum* species and composed of partially decomposed plant remains and secondary organic compounds made by microbes (secondary metabolite). *Sphagnum* mosses decompose much slower in comparison to sedges (*Carex*), lichens and other typical bog species (Wieder & Vitt, 2006). This commonly results in increasing fractions of *Sphagnum* material with depth (van Breemen, 1995). *Sphagnum* species resists decay and acidifies the environment through the release of phenolic compounds and carbohydrates (Charman, 2002). *Sphagnum* mosses have through their growth and production of decay-resistant litter formed large areas of boreal peatlands and occupy major areas of these. A low peat accumulating fen with high pH can quickly be converted into an acidic high peat accumulating bog when *Sphagnum* mosses start to grow (Wieder & Vitt, 2006). The *Sphagnum* species have different affinity to variously wet habitats, making them useful as a proxy for climate changes (Svensson, 1988b).

The most important time period for peat growth in the northern latitudes is the Holocene, which covers approximately the last 10 000 radiocarbon years (or 11 500 cal yr BP). The time scale in paleoenvironmental studies is critical, and the use of radiometric dating techniques provides an absolute timescale, which is useful when comparing different types of sites and sedimentary records (Charman, 2002). The radiometric dates can then be used in a peat accumulation model.

2.2 Atmospheric Dust

Peatlands are important archives of atmospheric dust deposition, and contain records of particulate deposition since peat formation began (Franzén, 2006). As plant remains accumulate on the peatland, dust deposited on its surface will be buried (Chesworth et al., 2006). Dry deposition onto peatlands can be of different origin: biogenic (seeds, pollen), phytoliths (biogenic silica), pedogenic (from soil erosion), oceanogenic (from salt spray), pyrogenic (smoke, ash from fires), plutogenic (volcanic ash), cosmogenic (meteorites, extra-terrestrial dust) or industrial dust (Shotyk, 1988). Ombrotrophic peat bogs generally have ash concentrations around 1-2 % but it can reach up to 15 % in fen peats (Franzén, 2006). Ombrotrophic *Sphagnum* peat have relatively low ash content as their nutrient supply depend fully on precipitation, dry deposition and their ability to recycle nutrients (Shotyk, 1988), while fens provide nutrients to the peat and can potentially impact nutrient-poor systems (Kylander et al., 2018). Climate act as the main control on the amount of dust in the atmosphere and fallout on land and in the oceans, which enable feedbacks between dust and climate (Franzén, 2006).

Prehistoric human impacts such as the use of fire, forest clearance and peat mining have left traces in the vegetation, charcoal and geochemical input from soil dust (Charman, 2002). However, recent anthropogenic activities have significant impact on the amount of dust in the modern atmosphere and could affect chemistry of surface peat (Franzén, 2006; Shotyk, 1988). Anthropogenic input of Sn, Cu, Cd, Zn, Hg and Pb greatly affect the concentrations in dry dust, while Al, Ti, Fe and Mn from anthropogenic sources are insignificant compared to natural levels. For example, concentrations of Pb from anthropogenic sources can be 350 times greater than from natural sources (Shotyk, 1988). Minerals found in peat are dominantly silicates and can be found as soluble biogenic silica from plants (authigenic) and insoluble crystalline quartz, orthoclase, plagioclase, mica and clays (allogenic). Although pyrite is not stable under the low pH conditions of bog surface waters (pH 4) and dissolved sulphur is a limited nutrient, sulphides are common at the bottom of mires (Shotyk, 1988).

Ashing of peat can be done to remove organic material from peat samples and temperatures between 500 and 550°C has been shown to do so efficiently (Sjöström, 2018). However, some elements are affected by ashing including aluminium that has displayed some decrease above 350°C, and concentrations of Na, S and Mg has been shown to decrease significantly. For elements of interest in this thesis (Al, Ti, Mg, Mn, K, P, Fe and selected trace elements) only minor losses have been reported. Combustion can also alter some minerals, such as iron oxides, sulphates and the more sensitive clay minerals, which is important to consider in mineral identification of ashed peat (Jenny K. Sjöström, personal communication, June 4, 2019).

2.3 Methods for the Characterization of Peat and Peat Ash

With infrared radiation (IR) spectroscopy, IR waves are sent through a medium, causing vibrations of the molecules with polar bonds therein. IR spectroscopy gives information about energy levels of the molecules in wavenumbers (cm^{-1}). The molecules are excited at different wavelengths, depending upon their structure and atomic composition. Consequently, the absorbance of IR occurs at molecule-specific wavelengths. The IR spectrum is a “fingerprint” of every molecule, which makes IR useful for characterizing a range of substances. IR spectroscopy is widely used for identification of complex organic macromolecules (e.g. humic substances) where the IR spectra of molecular structures and functional groups are associated to a range of absorption bands (Krumins et al., 2012; Niemeyer et al., 1992). Using Fourier Transform Infrared spectroscopy in the mid-infrared region (wavenumbers 4000-400 cm^{-1}) on peat produces data about functionals groups containing mainly C, O and H and how these are structured and related to each other (Krumins et al., 2012).

Different peat deposits can show large differences in their concentration of chemical elements and functional groups (Krumins et al., 2012). The mid-infrared region is used for studying principal band vibrations of organic and inorganic molecules (Colthup et al., 1990). The IR spectrum can be divided into two regions: wavenumbers $<1300 \text{ cm}^{-1}$ are in the fingerprint region, while wavenumbers $>1300 \text{ cm}^{-1}$ are in the functional group region (Ning, 2011). The absorption peaks or bands in the functional group region all generally are linked to a specific functional group, which enable peak interpretation. The fingerprint region reveals the presence of some functional groups as well as certain compounds.

Attenuated Total Reflection spectroscopy has been used since the 1960's and because it requires little or no sample preparation, is non-destructive and can be used for many different materials, ATR is today one of the most adaptable analysis techniques (Khoshhesab, 2012). The single-bounce-ATR produces a single internal reflection using a prism and is

suitable for strong absorbers, small sampling area and solid samples (Khoshhesab, 2012). A diamond prism is more expensive than other crystals, but very hard and chemically inert (however, highly acidic, caustic or small hard samples may cause damage to it).

X-ray fluorescence is a non-destructive analytical method with high resolution results that provides different elemental information on mineral chemistry. This is used in paleoclimate studies for understanding changes in atmospheric deposition, hydrology and potentially, biological productivity. Using only XRF elemental data for mineral dust analysis can involve limitations since minerals with similar chemistry can be difficult to discriminate and dust event can also vary mineralogically (Sjöström et al., 2018). Core scanning produces a micro-radiographic image and micro-X-ray fluorescence spectrometry elemental profiles. The radiation intensity is how many X-ray quanta that are emitted or measured per second. The XRF data are produced as peak areas and is a relative concentration measurement, yet the data is semi-quantitative which is useful for comparing spectral data from samples to get information about the relative elemental concentrations between samples (Bruker, 2019). The data is extracted by calculating the area under each peak.

2.4 Radiocarbon Dating

Radiometric dating build upon radioactive decay of isotopes. Since peat contains around 50% carbon, it is ideal for radiocarbon dating (Charman, 2002). Atmospheric ^{14}C has not remained constant over time, which results in radiocarbon years and calendar years are not the same. Nonetheless, this effect can be corrected for with a calibration curve for tree rings, and the corrected age is normally quoted cal yr BP or converted to the AD/BC timescale. The fluctuating atmospheric ^{14}C can lead to time periods with a plateau in the calibration curve, i.e. that a long time period in cal yr BP have the same radiocarbon age (Charman, 2002).

2.5 Late-Holocene Climate Variability

Holocene, the last interglacial, is described as a period of large and more frequent climate variations than what is previously recorded. It is suggested that both Earth's orbital variations and solar variability has been important factors impacting insolation to Earth throughout this period (Mayewski et al., 2004). During early and middle Holocene, the warm period known as the Holocene Thermal Maximum (HTM), gave relatively warm and dry summers in northern Europe. The HTM has been dated to 8000-4400 cal yr BP in southern Sweden (Seppä et al., 2009). This was followed by a cooling trend in the late Holocene and substantial climate shifts (Hass, 1996). The last 5000 years has showed a coupling between temperature and humidity proxies, i.e. relating warm anomalies with dry conditions and cold anomalies with humid conditions (Seppä et al., 2009).

The well-dated and high-resolution Greenland Ice Sheet Project Two (GISP2) glacier fluctuation record used Cl ion as a proxy for strong Icelandic low and thus strong westerlies over the North-Atlantic-Eurasian region, inferring a rapid climate change (Mayewski et al., 2004). The highest summer temperature anomalies are currently coupled to the anticyclonic circulation type. When the blocking anticyclone is in the most extreme form, high pressure systems becomes stationary over Scandinavia, causing weak westerlies and reduced precipitation. Seppä (2009) suggested from these evidence, that high summer temperature, low humidity and anticyclonic circulation can describe climate variability even at centennial-scale in northern Europe during the last 5000 years. The results from numerous pollen-based annual mean temperature reconstructions of Holocene climate variability in northern Europe were summarized by Seppä et al. (2009), giving the possibility to investigate regional climatic trends. For comparison, a bog surface wetness reconstruction from northern Finland

(Väliranta et al., 2007) and stacked peat-stratigraphical records from southern Sweden (Rundgren, 2008) are also used to describe climate variability during the late Holocene. During this time, the records show a gradual cooling trend, but with high temperature anomalies at 5000-4000, 3000-1000 and 100 cal yr BP and colder anomalies dating to 3800-3000 and 500-100 cal yr BP (Seppä et al., 2009).

At the end of the HTM (5000-4000 cal yr BP), climate reconstructions point to high temperatures and low humidity (Seppä et al., 2009). Thereafter, a cool and wet phase begins. Between 4200 and 3800 cal yr BP, the westerlies were generally weak and northern Europe experienced decreasing temperatures. The GISP2 proxy records show increasing westerlies again during 3500-2500 cal yr BP, which is linked to ice-rafting events in the North Atlantic (Bond et al., 1997; Mayewski et al., 2004). The bog surface wetness record associated lower temperatures to increased humidity around 3500-3200 cal yr BP (Väliranta et al., 2007) and Rundgren (2008) also observed a shift to wetter conditions in the stacked peat records, with a peak at 3300 cal yr BP.

During 3000-1000 cal yr BP (peak at 2000 cal yr BP) high temperatures from the pollen-based record are consistent with dry conditions in the bog surface wetness record (Hass, 1996; Väliranta et al., 2007). This period includes the historically documented Roman Warm Period (ca. 2000 cal yr BP) and the Medieval Warm Period (MWP, ca. 870-600 cal yr BP) (Hass, 1996). However, it is confirmed from the pollen-based records that the MWP is part of a longer warm period in northern Europe, with no clear peak (Seppä et al., 2009). Between 1200 and 1000, the GISP2 show a rapid climate change event which is associated with low temperatures in Europe and dominantly weak westerlies over the North Atlantic region (Mayewski et al., 2004). Thereafter, the climate became more unstable and show noteworthy temperature alternations (Hass, 1996). Temperatures were decreasing around 1000-800 cal yr BP with the onset of The Little Ice Age around 600 cal yr BP (Hass, 1996; Mayewski et al., 2004). This is consistent with the stacked pollen records, which display a cold anomaly dated to 500-100 cal yr BP (Seppä et al., 2009). During the last 150 years, the long-term cooling trend was reversed into a warming pattern, with mild winters and warm summers in northern Europe (Seppä et al., 2009). However, there are still few high-resolution records from the last 200 years because of complications in sampling and anthropogenic impacts (Mayewski et al., 2004).

3 Study Area

3.1 Site Description

The ombrotrophic peatland Store Mosse is located in southern Sweden (county of Jönköping). The bog has an approximate size of 77 km² and is situated around 160-170 m a.s.l. (Svensson, 1988a). The surrounding soils consists of glacial deposits where till and glaciofluvial sediments dominate (Svensson, 1988a). The area also show evidence of aeolian deposits in the form of dune ridge systems and sand sheets, but research about these is incomplete (Kylander et al., 2016; Svensson, 1988a). The north-western Store Mosse peatland is crosscut by an extensive dune ridge. The surrounding bedrock consists of metamorphosed felsic intrusive rocks, mostly granite and gneisses (1.7-1.8 Ga), with a mineralogy consisting of quartz, alkali feldspars, plagioclase feldspar, micas, amphiboles and a mixture of trace minerals. The bedrock outcrops in Store Mosse consists predominantly of granites, but includes a few lenses of mafic (gabbroid-dioritoid) rocks (“Berggrund 50 000-250 000 vektor” © Sveriges geologiska undersökning, 2019).

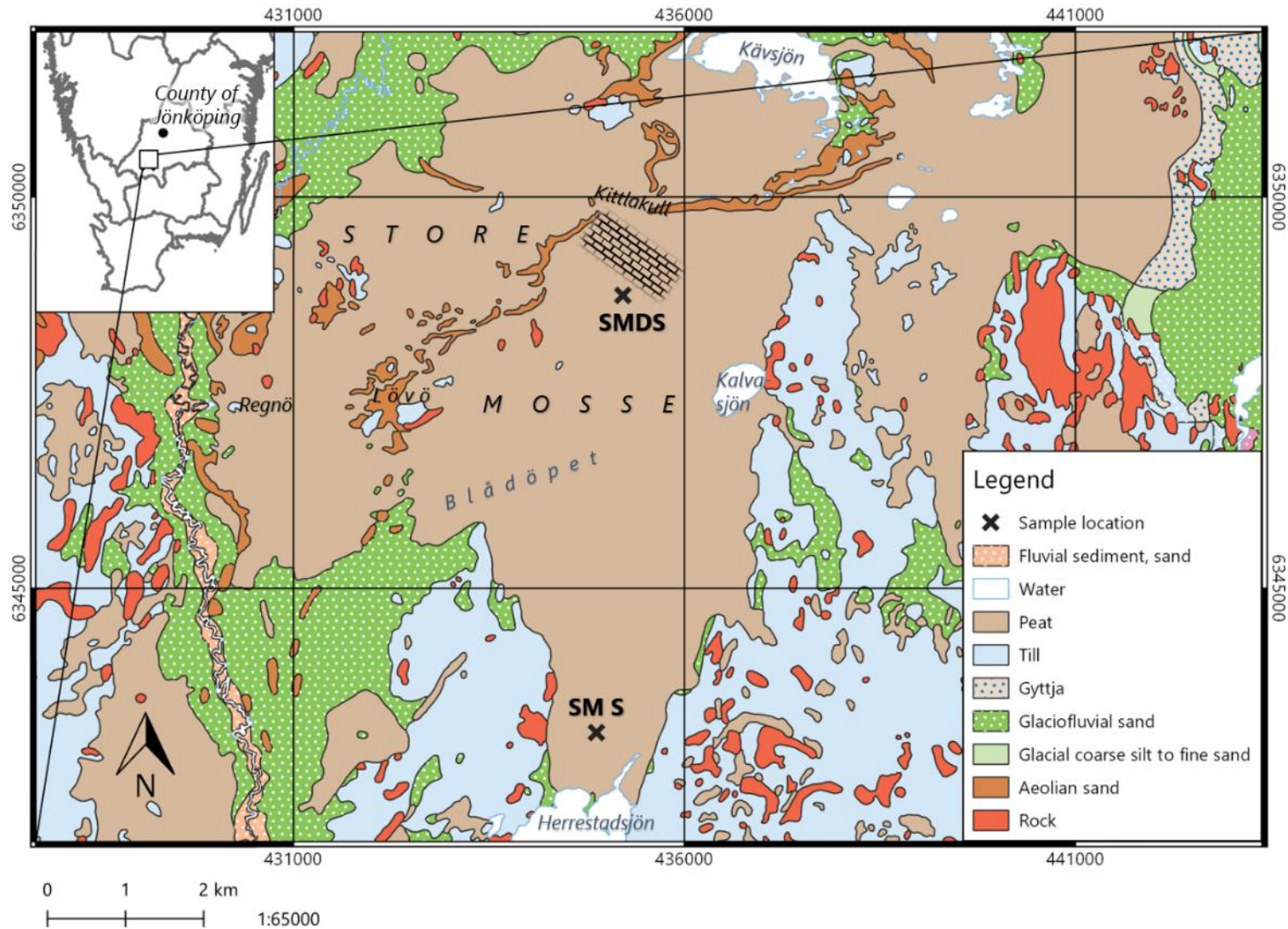


Figure 1. Deposit map of Store Mosse. The map shows different soil types in Store Mosse and its surroundings. Core sampling location for this project is labeled SMDS (Store Mosse Dune South) and previous core sampling location from Kylander et al. (2013) is labeled SM S (Store Mosse South). The squared area just north of SMDS core location has been used for peat cutting. "Jordarter 1:25 000 – 1:100 000 vektor" © Sveriges geologiska undersökning; "Översiktskartan vektor" © Lantmäteriet (2019).

The modern bog vegetation is quite complex and varied, yet it comprises most of the typical mire vegetation in South Swedish highlands today, which is mainly a mixture of sedge and moss capsules, dominated by *Sphagnum* species (*S. cuspidatum*, *S. papillosum*, *S. magellanicum* and *S. rubellum*), heather, crowberry and small pine trees (Svensson, 1988a). The sampling site is situated in the north-eastern part of Store Mosse national park, around 1 km southeast of the sand dune ridge and 3 km south of lake Kävsjön (Figure 1). The north-eastern part of Store Mosse has been used for peat mining during the beginning of the 20th century and occasionally display a decomposed peat surface due to ditching and peat cutting (Svensson, 1988b)

3.2 The Store Mosse Bog During the Holocene

The retreat of the Scandinavian Ice Sheet from Store Mosse occurred around 14400 cal yr BP. Store Mosse lies within the area that was once covered by the glacial ice-dammed lake (or lakes) Fornbolmen (Svensson, 1988a). The Store Mosse bog together with the lakes Bolmen, Vidöstern, Flåren and Furen today make up the remains of the glacial lake (Kylander et al., 2016). Due to isostatic uplift the lake was drained southwards, exposing the former lake bottom and wind erosion resulted in numerous dunes and sand sheets in the Store Mosse bog area and west of the bog (Kylander et al., 2018). When the lake had drained, initiation of peat formation occurred on the open sandy areas in the northern part of the former lake. This paludification process is not seen in the eastern southern Sweden, where peat formation is started with infilling of a lake (Svensson, 1988a).

The peatland development in southern Store Mosse has been described with an initial fen stage followed by three bog stages (Malmer et al., 1997; Svensson, 1988a). Macrofossil analysis is required to properly define stage boundaries, yet large bulk density decreases should imply a shift in stage (Kylander et al., 2013). Between 6000 and 5000 cal yr BP, the northern part of Store Mosse was covered with sandy areas and occupied by fen vegetation (mainly *Carex* species). The *Fuscum* and the *Rubellum-Fuscum* bog stages are both initiated with slightly humified peat which continuously is replaced by highly humified peat, something that has been observed all over the bog. These shifts in peat decomposition seemingly depend on water table fluctuations and other environmental conditions, due to changes in climate. A dry climate generally form highly humified peat layers, while a wet climate would yield less humified layers (Svensson, 1988a).

3.3 Climate and Storminess Affecting Store Mosse

The county of Jönköping is situated in the southern Fennoscandia approximately in the middle of the continent. The prevailing wind direction is subject by the westerlies and the climate is temperate with cool summers and quite mild winters, giving an average annual temperature of 6 °C and around 700 mm of annual precipitation (Björck & Clemmensen, 2004; Kylander et al., 2013). Climate at the mid-latitudes in the North Atlantic region, including the Arctic region and north-western Europe, is strongly affected by the North Atlantic Oscillation (NAO). The NAO is based on atmospheric pressure differences between the Icelandic low and the Azores high (Olsen et al., 2012) and it influence the strength and direction of westerly winds and where storms travel (storm tracks) in the North Atlantic. Variations in temperature and precipitation in the region are influenced by the NOA, which has been shown to affect ecosystem behaviour and growth seasons (Olsen et al., 2012).

Westerly storms contributed to dust deposition before human population increased in the Scandinavian peninsula and gave marine influx of Cl, Na, K, Mg, Ca, Sr, B and I (Franzén, 2006). The frequency and intensity of storms (storminess) during the winter in Europe is

affected by the jet stream and atmospheric pressures over the North Atlantic (Orme et al., 2016). Increased storminess can activate aeolian deposits (Sorrel et al., 2012). Also modern desert dust is reported during strong southerly winds which occur periodically 1-10 times during a 50-year period, whereas the older parts of the peat core can preserve dust from loess originated from remote areas of Sweden and from NW China (Franzén, 2006). In their study on two raised bog peats in the province of Halland, Björck & Clemmensen (2004) used quartz grains >0.2 mm (aeolian sand influx) as a proxy for winter storminess and linked variations on decadal-scale to variations in the storm tracks in the North Atlantic during winter, while centennial-scale changes were coupled to frequency and severity of cold and stormy winters.

4 Analytical Materials and Methods

4.1 Sampling

Sampling was made on September 15, 2018 in north-eastern Store Mosse ($57^{\circ}16'37.70''\text{N}$, $13^{\circ}55'30.86''\text{E}$, see Figure 1). The core Store Mosse Dune South (SMDS) was recovered using a Russian corer (diameter 7.5 cm) and consist of six 1-m sections, overlapping each other by 25 cm, taken to a depth of 450 cm from two alternating holes. Changes in the bulk density were used for core alignment. The SMDS core was sub-sampled in continuous 1 cm thick slices using a stainless-steel knife. The samples were put in pre-weighed plastic zip-bags and weighed (wet weight). The sample slices were frozen at least 24 hours prior to freeze-drying. All 591 samples were freeze-dried for 4 days to remove all water content. For details on the freeze-drier and its pump, see Appendix, Table 8.

4.2 Analyses

4.2.1 X-ray Fluorescence Core Scanner (XRF-CS)

In November 26-28, 2018 XRF-CS analyses were performed on the SMDS core using an ITRAX™ core scanner at the Department of Geological Sciences, Stockholm University, Sweden. The analyses on wet core sections was performed for characterization of the sedimentary environment and to allow for correlation of cores within the same site (quantification of changes in sample density). These analyses were done at voltage 30 kV, current 40 mA, step size 0.5 μm and exposure time of 50 seconds. XRF-CS analyses were also carried out on March 8 and 20, 2019 on ashed SMDS peat samples packed in sample boats. Labware was cleaned with ethanol between each sample. The sample boats are specially built for the analysis purpose and have inner measurements of approximately 8 mm length, 2 mm width and 2 mm depth (Figure 2). The XRF-CS analyses on discrete ashed samples was done at voltage 30 kV, current 50 mA, step size 0.5 μm and exposure time of 25 seconds.

4.2.2 Bulk Density, True Depth and Ash Content

The bulk density of peat is highly dependent on the mineral content and the degree of compaction. Since peat mainly consist of organic material, the measurement is organic bulk density. Henceforth, bulk density is used to calculate accumulation rates and to make compaction estimates. It is also used for identification of major deposit transitions (fen-bog boundary) and significant shifts in decomposition.



Figure 2. The images show the ashed sample boats prepared for XRF-CS analysis (left) and a dried peat sample during tracing for bulk density measurements (right).

The samples were weighed again after freeze-drying (dry weight), and the bag weight was subtracted from the dry weight. Since the core has an uneven surface and does not completely fill the core tube, the bulk density must be calculated separately for each 1 cm-sample slice. The total filled area of the 7.5 cm wide core tube was calculated to 22.089 cm², and the filled area was cut out on white paper and weighed as reference (0.1728 g). Because of variation from sub-sampling, all samples were then traced with a pencil on white pieces of paper and their thickness was estimated (Figure 2). The traces were cut manually and weighed. The bulk density (g/cm³) was then calculated by dividing the dry weight of each sample with its estimated volume. Bulk density measurements and images of the fresh cores were used to calculate the true depth of the subsamples and for core alignment. The total compiled depth, or true depth, after core alignment was 427 cm.

For every 5 cm in the compiled core, milling was done ($n = 81$) at 30 strokes per second for 2 minutes using an ESSA Lab Wizz plant mill equipped with Teflon vials and agate milling balls. Silicon gloves were used and all labware were cleaned with ethanol between each sample. Lastly, dry ashing was performed at the Department of Geological Sciences at Stockholm University, Sweden. The crucibles were pre-dried at 105°C for at least 4 hours, placed in desiccator to cool and then weighed. An additional 81 samples were chosen so that ashed samples were at every 2 or 3 cm throughout the compiled core. The samples ($n = 162$) were placed in crucibles and dried for at least 4 hours at 105°C. The crucibles with sample were then cooled in desiccator and weighed again. Thereafter, the samples were thermally combusted at 500°C for 4 hours, placed to cool and then weighed again (ashed sample weight). The ash content was calculated from the ashed sample weight as a percentage of the dry weight and shows the amount of inorganic material present in the sample.

4.2.3 Attenuated Total Reflection Fourier Transform Infrared (ATR-FTIR) Spectroscopy

Bulk peat ($n = 81$) and ashed peat ($n = 162$) samples were analysed by Fourier Transform Infrared spectroscopy, using a Thermo Scientific™ FTIR equipped with an iS7 ATR device with a single-reflection diamond crystal at the Department of Geological Sciences at Stockholm University, Sweden. For specifics on the ATR, see Appendix, Table 7. Labware and the ATR-diamond was cleaned with ethanol between each sample. The measurements were obtained for the mid-infrared wavelength spectral range of 4000-400 cm⁻¹ (2.5-25 μm).

4.2.4 ¹⁴C Radiometric Dating and Age-depth Model Construction

Three samples were picked for macrofossils and analysed with Accelerator Mass Spectrometry (AMS) radiocarbon dating at the Tandem Laboratory, Uppsala University, Sweden. The age-depth model for the SMDS core was based on three radiocarbon dates and built using the Bacon program v.2.2 (Blaauw & Christeny, 2011) which uses Bayesian statistics. With millions of iterations, the model chooses average values appropriate for the age-depth model and is suitable for few dates. The radiocarbon dates were calibrated using the IntCal13 calibration curve (Reimer et al., 2013). Further statistical information about the age-depth model is given in Appendix, Table 9 and Figure 15.

4.3 Statistical Analyses

4.3.1 ATR-FTIR Data Reduction

The ATR-FTIR absorbance values for all bulk and ashed peat samples were compiled, normalised and reduced to peaks with the SDP package (Álvarez-Fernández & Martínez-Cortizas, 2019) using the statistical software R (R Core Team, 2013). The normalization converted the data to standard scores (or z-scores), which show the distance in number of standard deviations that an observation is from the mean (Weiss, 2013). The second derivative of the absorbance values was also calculated in the SDP script and are a measure for the sensitivity of the absorbance at every wavenumber. Therefore, the second derivative is useful for locating absorbance peaks that have high sensitivity in the spectra. Not all peaks in the spectra are relevant for this thesis and therefore the most interesting peaks were selected from the second derivative. In order to process the spectra, one can use a multivariate analysis, such as principal component analysis, to interpret it.

4.3.2 Principal Component Analysis (PCA)

The purpose of using a PCA is to explain a major part of the variance among the samples with less factors than initially and to identify major trends in the data. PCA was performed on the transposed data matrix of the ATR-FTIR data for bulk and ashed samples separately. Also, PCA was applied to the standard scores of XRF-CS elemental data of the discrete ashed sample boats. The choice of numbers of components (factors) was based on the total variance in the data (>85%), the Kaiser threshold (eigenvalues <1) and the value of interpretation and relevance for this thesis.

The PCA was performed using JMP v.14 software (SAS Institute Inc., 2019) with a varimax orthogonal rotation. A rotation redistributes the factor loadings over the factors. More specifically, the orthogonal rotation of the loading matrix will change the component variances, but the components remain uncorrelated and variable communalities (rotated factor loadings) are preserved. The varimax rotation, which is the most popular orthogonal method, attempts to maximize variance for the squared values of factor loading for each factor.

5 Results

Bulk density, ash content, PAR, spectral data from ATR-FTIR analyses for bulk and ashed samples and (relative) elemental data from XRF-CS analyses have been acquired for the SMDS peat. Statistical handling of these include age-depth modelling using the R package Bacon, PCA on ATR-FTIR data for both bulk and ashed samples and PCA on the XRF-CS elemental data. The number of extracted factors for each PCA and the total variance explained by the factors are shown in Table 1. For PCA on the ATR-FTIR data, the main positive loading peaks are representing high absorbance within certain spectral bands. These can be related to a chemical component. However, every compound has several vibrations and they may overlap with vibrations of another component.

Table 1. Summary of the PCA. BP and AP stand for bulk and ashed peat, respectively, while XP stands for the XRF-CS data.

Samples	Extracted factors	Total variance explained (%)
ATR-FTIR bulk peat	BPC1-BPC4	90.3
ATR-FTIR ashed peat	APC1-APC4	93.3
XRF-CS ashed peat	XPC1-XPC4	87.4

5.1 Store Mosse Dune South (SMDS) Age-depth Modelling

The SMDS core consists entirely of dark brown *Sphagnum* peat, which varies from fresh *Sphagnum* mosses at the top to highly decomposed peat at the bottom. The results from the three radiocarbon dates and details of the material dated are given in Table 2, including the median probability of the 1σ range and errors from the analytical software. The SMDS core covers the last 4825 cal yr BP. The age-depth model was created from the known age of the modern bog surface at 0 cm and the three radiocarbon dates (Figure 3).

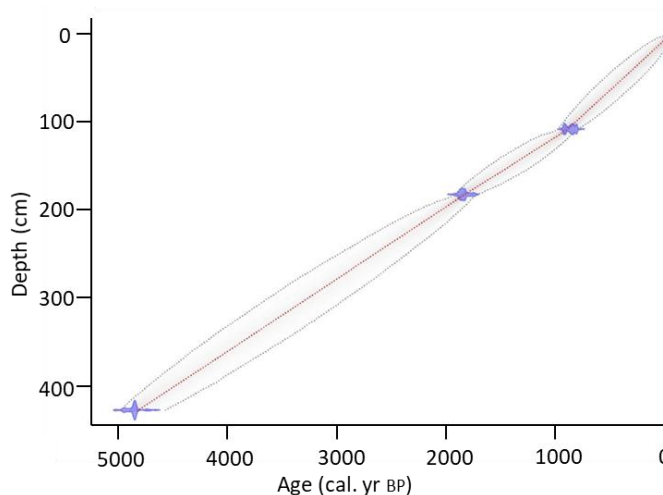


Figure 3. Age-depth model obtained from three radiocarbon dates using the Bacon package (Blaauw & Christeny, 2011) in the statistical software R.

Table 2. Radiocarbon measurements from Store Mosse Dune South core. Ua = Tandem Laboratory, Uppsala University, Sweden.

Sample name	True depth (cm)	Laboratory no.	Dated material	$\delta^{13}\text{C}$ ‰ V-PDB	^{14}C yr $\pm 1\sigma$	Calibrated age range (cal yr BP)
SMDS C2-72	108	Ua-61551	Seeds, <i>Sphagnum</i> species	-25.4	961 \pm 29	796-930
SMDS C3-71	182	Ua-61552	<i>Sphagnum</i> species	-24.9	1897 \pm 29	1737-1918
SMDS C6-98	426	Ua-61510	Insect remain, <i>Eriophorum</i> species	-25.5	4292 \pm 35	4826-4961

5.2 Organic Bulk Density, Ash Content and PAR

Bulk densities vary between 0.033 and 0.14 g/cm³, with an average value of 0.066 g/cm³ ($n = 408$; Figure 5). The bulk density values are high at the bottom of the profile and increase to reach the maximum value of 0.14 g/cm³ around 4600 cal yr BP. This is followed by a gradual decrease in bulk densities until 4200 cal yr BP, from when the values remain stable for 400 years. Around 3600 cal yr BP the values rapidly increase to a peak maximum of 0.12 g/cm³ at 3500 cal yr BP, and shortly thereafter values quickly decrease again. The following 1000 years show minor increases at 3250, 3030 and 2640 cal yr BP. Around 2500 cal yr BP bulk density values increase and are maintained high until 2150 cal yr BP. The values then slightly decrease over more than 600 years, until decreasing rapidly at 1530 cal yr BP and reaches the lowest values of 0.033 g/cm³ at 1355 cal yr BP. Lastly, the profile shows three significant peaks from the baseline with increases at 1050, 840 and 520 cal yr BP, and then the values increase steadily over the last 350 years.

The ash content is low for the majority of the peat profile with an average value of $1.1 \pm 1.7\%$ (2σ ; $n = 162$). The one exception is the value of 7.1% at 3775 cal yr BP standing out from the rest. At the base of the profile, the ash content shows a small peak centred on 4620 cal yr BP at 2.0%. Values are also higher at the very top of the profile (last 300 years) with values up to 5.2% (Figure 6).

The net PAR varies between 25 and 125 g/m²/yr and the average is 59 ± 39 g/m²/yr (2σ ; $n = 406$). At the base of the profile, PAR values are increasing and reach >110 g/m²/yr at 4600 cal yr BP (Figure 5). PAR values then gradually decrease until 4200 cal yr BP, from when they remain low for over 600 years. Around 3600 cal yr BP, the values rapidly increase and decrease, and this sharp peak is centred around 3500 cal yr BP (102 g/m²/yr). This is followed by another relatively stable period with low values for 950 years and minor increases occur at 3250, 3030 and 2640 cal yr BP. The PAR values start to increase around 2500 cal yr BP and the profile shows a broad peak with highest values at 2150 cal yr BP (85 g/m²/yr). Thereafter, PAR values remain stable or slightly decrease for almost 600 years until they start to decrease rapidly down to the lowest profile value of 25 g/m²/yr at 1355 cal yr BP. This is followed by three significant increases from the baseline at 1050, 840 and 520 cal yr BP and over the last 350 years the values gradually increase.

5.3 Principal Component Analysis on ATR-FTIR Data

The results of the ATR-FTIR analyses on ashed peat samples initially showed negative absorbance values for a substantial number of wavenumbers, which resulted in rerun of all ashed peat samples. ATR is a surface technique, which require a homogeneous sample surface, completely dry samples and cleaning of the crystal between analyses is critical to produce accurate results. The negative absorbance values could have resulted from insufficient contact between the sample and the ATR crystal or insufficient cleaning between analyses (Khoshhesab, 2012).

The absorbance spectra from ATR-FTIR analyses on the SMDS bulk and ashed peat samples including the average spectra are displayed in Figure 4. The second derivative of the absorbances was used to select relevant peaks for the principal component analysis and are displayed together with the average absorbance in Appendix, Figure 16 and Figure 17.

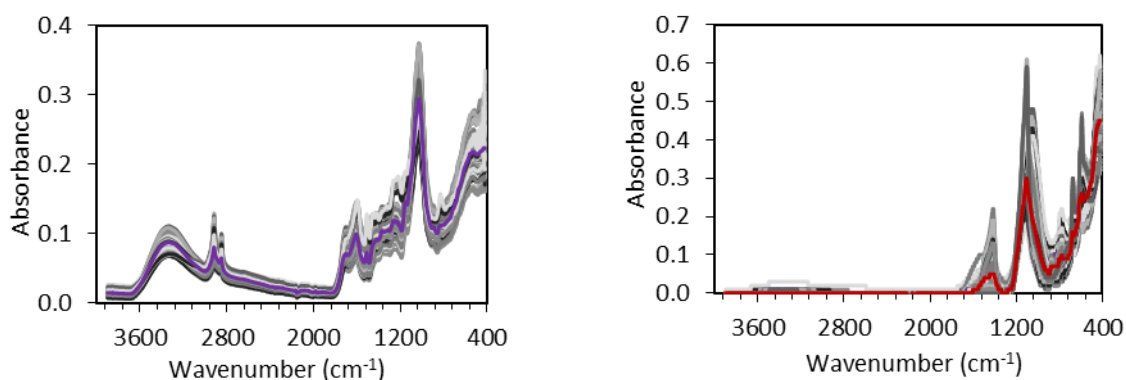


Figure 4. ATR-FTIR spectra for the SMDS bulk peat samples (left) and ashed peat samples (right). The purple and red lines show the average spectrum.

5.3.1 Bulk Samples

The PCA on ATR-FTIR bulk SMDS samples extracted four factors (BPC1-BPC4) which account for 90.3% of the total variance in the data. The factor scores and rotated factor loadings for the factors are presented in Figure 5 and Figure 9, respectively. The relative importance of each of the selected peaks can be shown for each factor by using commonalities (squared factor loadings), which facilitates interpretation of the different factors (Figure 7). BPC1 (38.1% of the total variance) show high factor loadings for absorption peaks at wavenumbers 2918, 2850, 2500-2000, 1736-1157, 839 and 719 cm^{-1} and negative loading for 3905-3633, 1059 and 1032 cm^{-1} . The factor scores for BPC1 decrease from the bottom until ca. 4200 cal yr BP when they stabilize around average values until ca. 2000 cal yr BP when they decrease further. BPC1 factor scores are moderately correlated with age ($n = 82$; $r = 0.45$).

BPC2 (33.8% of the total variance) shows factor loadings almost opposite of BPC1, except for lower wavenumbers. However, the factor scores are more variable with depth and does not show any significant correlation with age. If the factors loadings are compared to those of BPC1 (Figure 9), one can see that wavenumbers 3905-3633 and 2050 cm^{-1} have relatively high factor loadings, while 895, 839 and 719 cm^{-1} have relatively low loading on the factor. BPC3 (10.1% of the total variance) have positive factor loadings for wavenumbers 3905-3633, 895, 719 and 559-420 cm^{-1} . Moderately negative loadings are shown for 1059 and 1032 cm^{-1} as well as for 1736 and 1720 cm^{-1} . The factor scores are quite variable throughout the core. BPC4 (8.3% of the total variance) show high factor loadings for wavenumbers 2918, 2850, 1736, 1720 and 1705 cm^{-1} . Negative factor loadings are seen for 667 and 559 cm^{-1} . The factor scores for BPC4 have distinct decreases at 4300, 4000 and 3555 cal yr BP.

5.3.2 Ashed Samples

The PCA on ATR-FTIR analyses on ashed SMDS samples extracted four factors (APC1-APC4) which account for 93.3% of the total variance in the data. A comparative diagram for the commonalities is shown in Figure 8. The factor scores and the rotated factor loadings are displayed in Figure 6 and Figure 10, respectively. APC1 (31.2% of the total variance) have highly positive factor loadings for absorption peaks at 1203, 1163, 1147, 1101, 677, 646, 611, 594 and 563 cm^{-1} while 876, 451, 436 and 420 cm^{-1} have negative factor loadings.

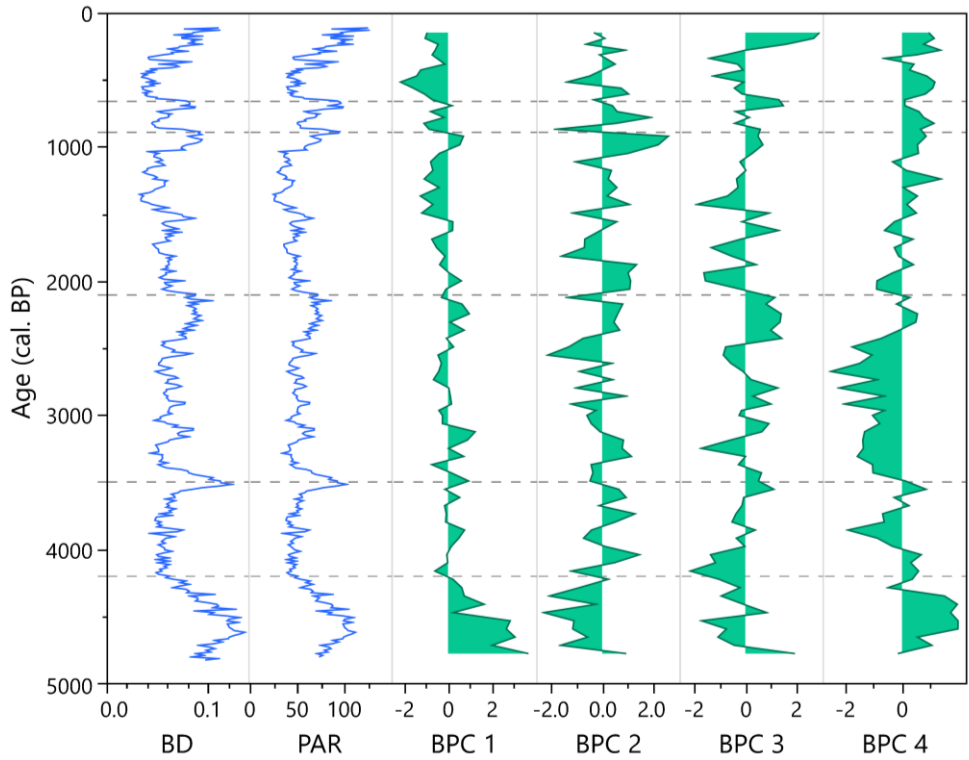


Figure 5. Organic proxies for the SMDS core with age (cal yr BP). The diagram presents bulk density (BD) in g/cm^3 , PAR in $g/m^2/year$ and factor scores for PCA on FTIR-ATR bulk samples (BPC1-BPC4). The horizontal dotted grey lines show significant decreases in bulk density values at 4200, 3500, 2100, 890 and 660 cal yr BP.

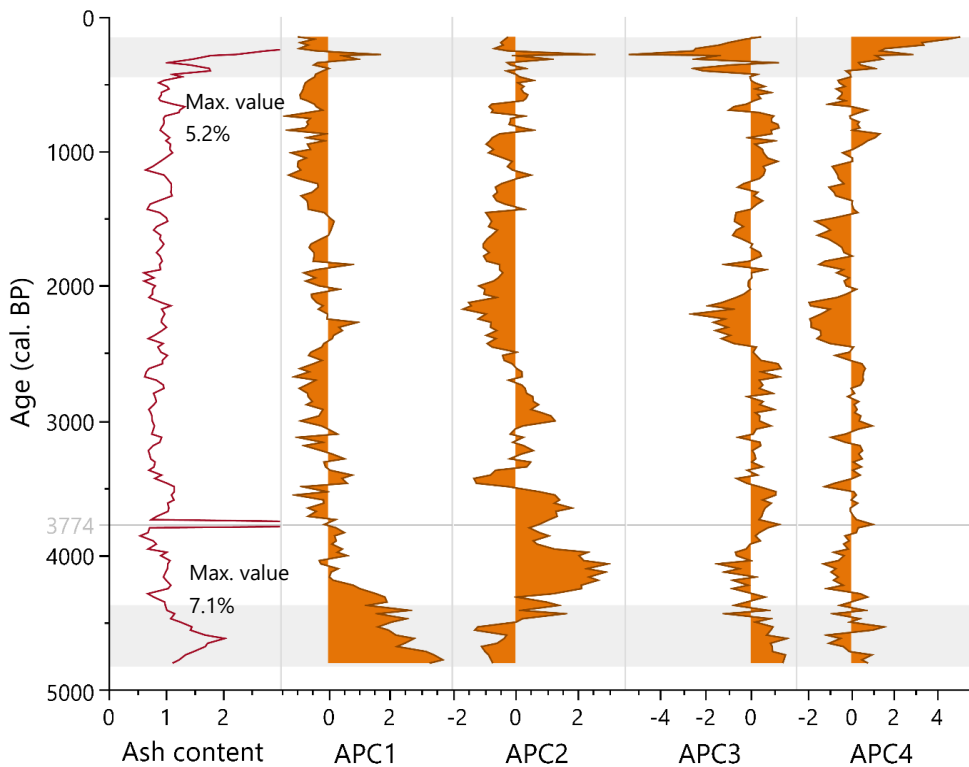


Figure 6. Inorganic proxies for the SMDS core with age. The inorganic data shows ash content as percent ash and the factor scores from the PCA on ATR-FTIR ashed SMDS samples (APC1-APC4). The grey areas show age regions with relatively high ash content (4830-4375, 3775 and 445-150 cal yr BP). Note that the scale of the ash content has been cropped to 3 % to more clearly show the variation in ash content over the main profile.

The factor scores are highly positive between 4800 and 4190 cal yr BP and then generally shows negative values. Other positive age ranges occur at 4000-3800, 3470-3405, 3290, 2330-2270, 2025, 1840 and 315-280 cal yr BP. APC2 (26.3% of the total variance) has highly positive factor loadings for 1510, 1495, 1477, 1412 and 513 cm^{-1} , while negative factor loadings are displayed for 993, 958, 798, 779, 714 and 677 cm^{-1} . The factor scores for APC2 show negative values from the bottom until 4535 cal yr BP when a shift occur to highly positive scores for 1000 years. Another negative peak occurs around 3430 cal yr BP, followed by positive scores between 3000 and 2735 cal yr BP. Between 2555 and present the scores are predominantly negative, except for a significant peak at 280 cal yr BP. APC3 (21.2% of the total variance) has positive factor loadings for 3691, 3678 and 3653 cm^{-1} and negative factor loadings occur at 876, 798, 779 and 714 cm^{-1} . Between 4800 and 4475 cal yr BP the factor scores for APC3 are positive but are followed by several negative peaks. The period 3900-2455 cal yr BP show largely positive factor scores and thereafter the scores rapidly become highly negative until 2060 cal yr BP. Thereafter, the factor scores are fluctuating between positive and negative until the last 400 years which again show highly negative factor scores for APC3. APC4 (14.5% of the total variance) has positive factor loadings for 1078, 1032, 1014, 993 and 958 cm^{-1} and negative factor loadings for 646, 611, 563 and 513 cm^{-1} . The factor scores for APC4 fluctuates for the lower part of the profile between positive and negative scores but shift to negative at 2455 cal yr BP. Positive scores are seen at 945-695 cal yr BP and then the scores significantly increase the last 380 years.

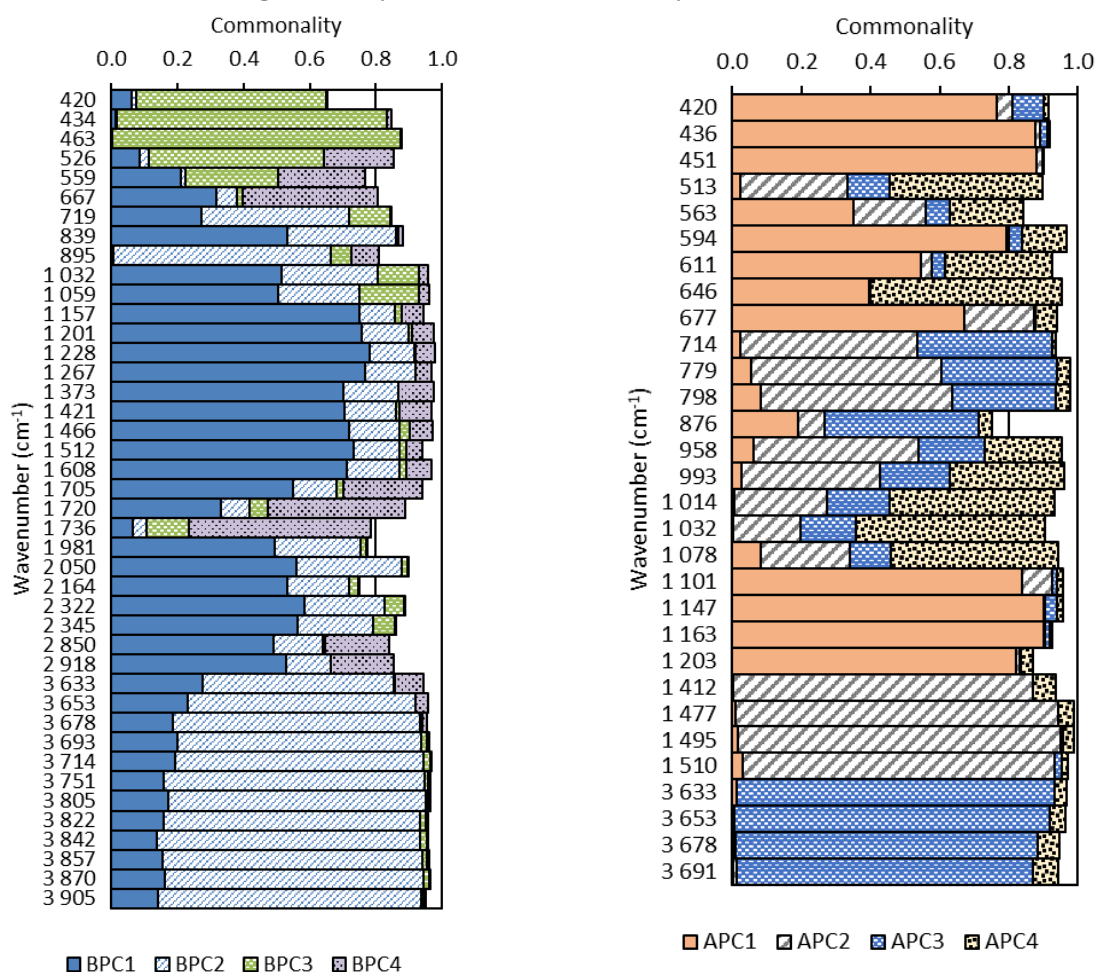


Figure 7 (left). Commonalities for the factors BPC1-BPC4 from the PCA on SMDS bulk ATR-FTIR samples. Figure 8 (right). Commonalities for the factors APC1-APC4 from the PCA on SMDS ashed ATR-FTIR samples.

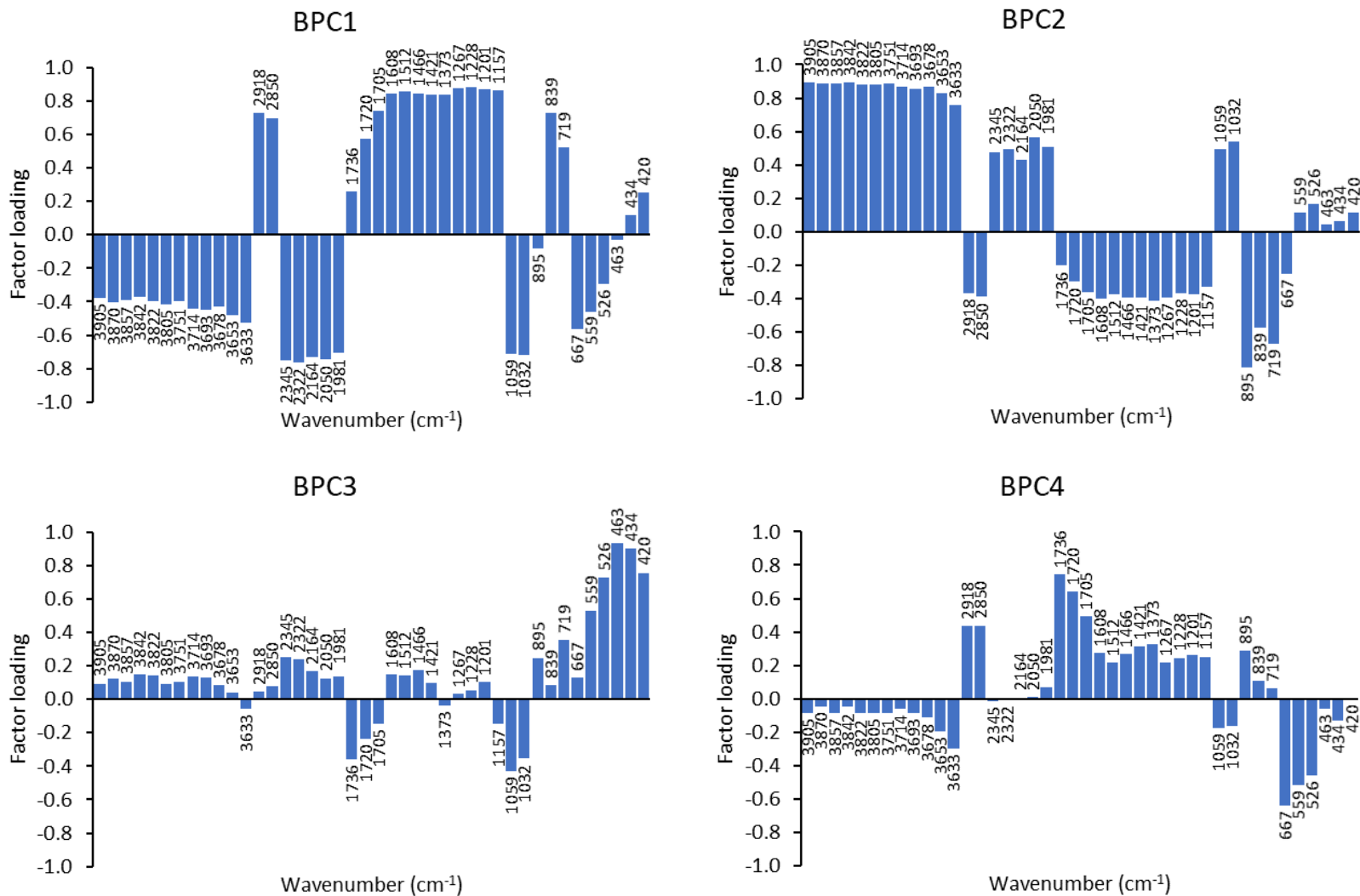


Figure 9. Bar charts of rotated factor loadings for the selected peaks of the SMDS bulk peat samples. The loadings are a result of the PCA on ATR-FTIR rotated data matrix, and show the results for factors BPC1-BPC4. The wavenumber that correspond to each selected absorption peak is shown next to the bar. Highly positive or negative factor loadings show a strong positive or negative correlation between the factor and the wavenumber.

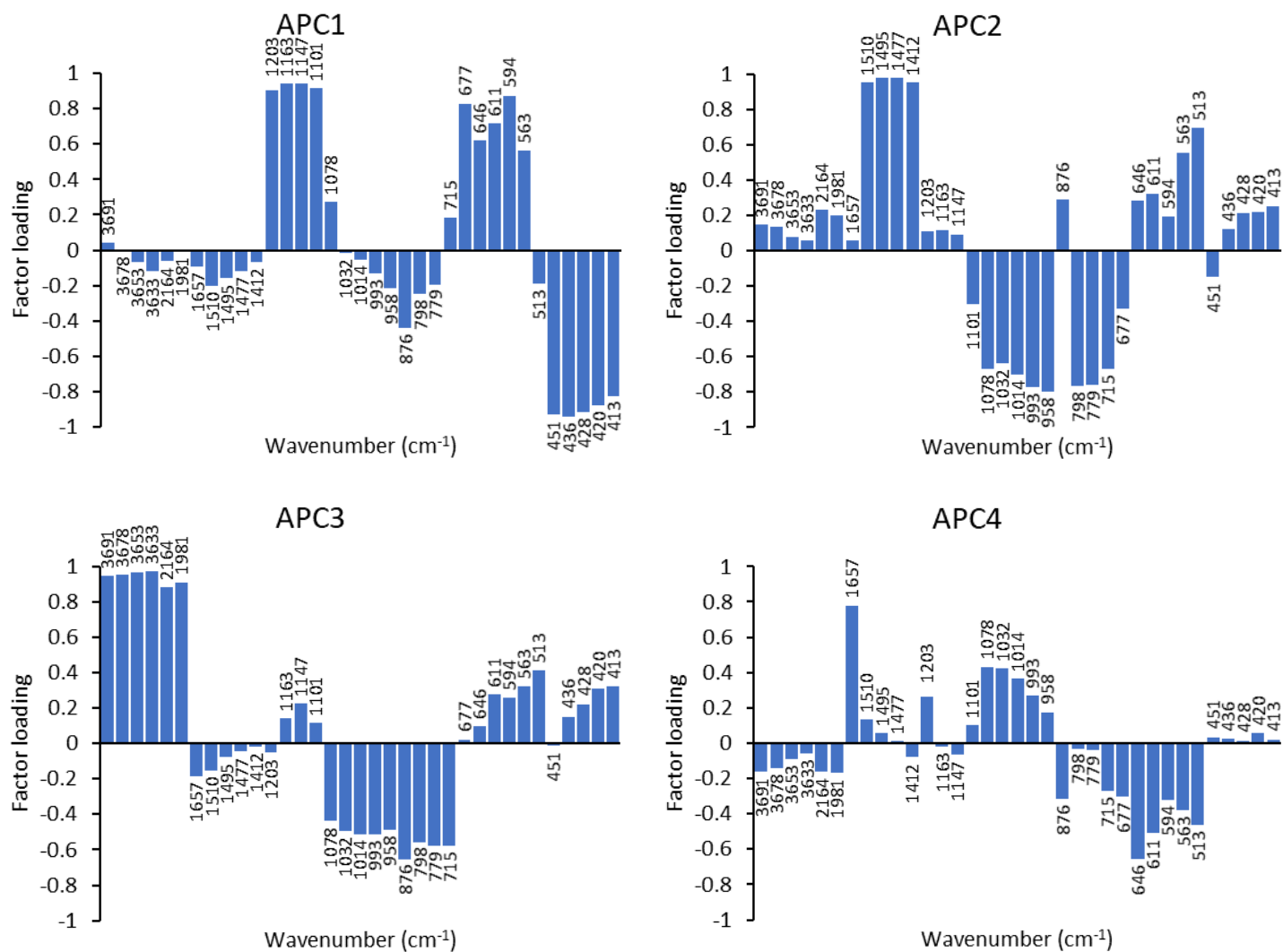


Figure 10. Bar charts of rotated factor loadings for the selected peaks of the SMDS ashed peat samples. The loadings are a result of the PCA on ATR-FTIR rotated data matrix, and show the results for factors APC1-APC4. The wavenumber that correspond to each selected absorption peak is shown next to the bar. Highly positive or negative factor loadings show a strong positive or negative correlation

5.4 Elemental Data from X-ray Fluorescence Core Scanning (XRF-CS)

The elemental data from the XRF-CS analyses is given as peak areas. The data is semi-quantitative and provides relative changes in elemental concentrations. Elemental profiles for the SMDS ashed samples for elements Al, Si, P, K, Ca, Ti, Mn, Fe, Cu, Zn, Br, Rb, Sr, Y, Zr and Pb with depth are shown in Figure 18, Appendix. The PCA on the elemental data from XRF-CS analyses extracted four factors (XPC1-XPC4) that explain 87.4% of the total variance in the data Table 3. Elements included in the PCA were Al, Si, P, K, Ca, Ti, Mn, Fe, Cu, Zn, Zr and Pb. Strontium and yttrium were excluded because they were put alone in one factor, meaning that the factor and the element is showing the same thing and is not useful for the PCA. Bromine and rubidium were also excluded from the PCA. The four factors in the PCA describe 87.4% of the total variance in the data. The rotated factor loadings and the factor scores can be found in Table 3 and Figure 11.

Table 3. Rotated factor loadings from the PCA on XRF-CS elemental data on discrete ashed SMDS samples for the factors XPC1-XPC4. The blue shade indicates the elements with high loading on the factor.

Factor	XPC1	XPC2	XPC3	XPC4
Variance	3.0	3.0	2.6	1.9
Percentage	25.1	24.6	22.0	15.7
Cumulative %	25.1	49.7	71.7	87.4
Variable	XPC1	XPC2	XPC3	XPC4
Zn	0.92	0.04	0.13	0.08
Pb	0.83	-0.10	0.35	-0.04
Si	0.72	-0.17	0.57	0.25
Cu	0.51	-0.51	0.38	0.27
Al	0.44	-0.02	0.63	0.52
Fe	-0.19	0.94	-0.05	-0.10
Mn	0.31	0.91	-0.04	-0.08
Ca	-0.22	0.84	-0.26	0.19
Zr	0.21	-0.18	0.92	0.00
Ti	0.33	-0.16	0.77	0.42
P	-0.06	0.10	0.09	0.91
K	0.38	-0.38	0.32	0.64

Factor XPC1 (25.1% of the total variance) shows high factor loadings for Zn, Pb, Si, Cu and Al. This factor has positive factor scores around 2870 and 700 cal yr BP and show highly positive scores for the last 350 years. Factor XPC2 (24.6% of the total variance) shows high factor loadings for Fe, Mn and Ca and factor scores are high at the bottom of the profile and are decreasing until ca 4000 cal yr BP when they shift to predominantly negative, except for another positive peak at 315 cal yr BP. Factor XPC3 (22.0% of the total variance) shows high factor loadings for Zr, Ti, Al and Si, and the factor scores display high variability. At the bottom, the factor scores are high until ca. 4500 cal yr BP and thereafter they show negative values for almost 1000 years when a sharp peak occurs. Between 3500 and 2500 cal yr BP the scores are negative again and the last 2500 years show alternating positive and negative peaks at centennial scale. Factor XPC4 (15.7% of the total variance) shows high factor loadings for P, K, Al and Ti. The factor scores are very variable but can be generalised into three stages. First, the factor scores are negative from the bottom to 4500 cal yr BP when a short period of positive scores occurs but is followed by an additional 800 years of negative scores. Between 3500 and 1000 cal yr BP the factor scores alternate greatly but are largely positive. At 1050 cal yr BP there is a sharp negative peak and it is followed by another negative peak between 650 and 400 cal yr BP.

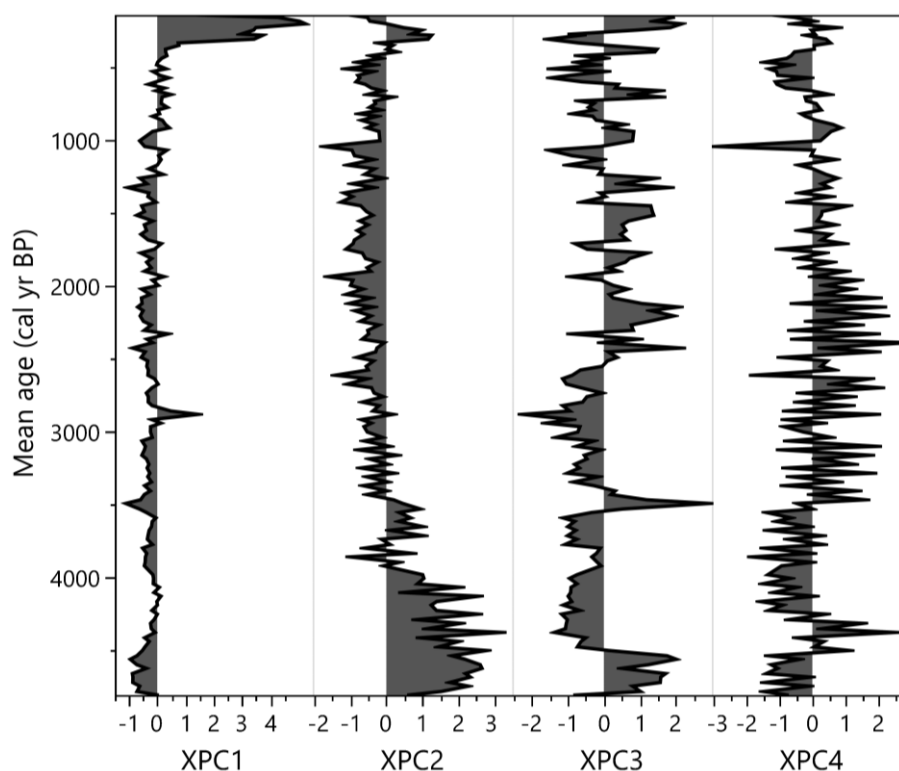


Figure 11. The plot shows the factor scores from the PCA on XRF-CS analyses of ashed discrete SMDS samples with age (cal yr BP) for factors XPC1-XPC4.

6 Discussion

6.1 Peatland Development

Changes in peat decomposition and humification are greatly affected by hydrologic changes (Björck & Clemmensen, 2004) and therefore the organic bulk density is considered a proxy of bog surface wetness and consequently effective humidity at Store Mosse. This information can be used in conjunction with the ash content and PAR data to identify major changes in the bog development. The bulk density range (0.033-0.137 g/cm³) and net PAR values (25-125 g/m²/yr) found in the SMDS sequence (Figure 5) are similar to those found in previous studies at Store Mosse by Kylander et al. (2013) (0.017-0.15 g/cm³ and 13-189 g/m²/yr) and by Svensson (1988a) and Malmer et al. (1997) (0.030-0.12 g/cm³ and 25-205 g/m²/yr). The core depth of 427 cm for the SMDS core is in line with earlier depth measurements of 4-5.5 m in the northern bog (Svensson, 1988a), suggesting that the northern part of Store Mosse has less massive peat successions than the southern part (Kylander et al., 2013). The mineral soil was however, not reached in the SMDS core.

The age-depth model for Store Mosse (Figure 3) is built on three radiocarbon dates and captures the main trend in the peat accumulation. However, the period around 5500-4500 cal yr BP has shown very high accumulation rates in the southern bog area, where the age-depth model was based on 14 radiocarbon dates covering 8500 years of peat accumulation (Kylander et al., 2013). Since the age-depth model for the lower part of the SMDS peat sequence only is based on one radiocarbon date, it can be concluded that any accumulation rate changes beyond a linear model is not captured by the current model. Additional

radiocarbon dates are required to fully understand the peat accumulation rates in the northern site as well.

The ash content (Figure 6) show similarities with the characteristic “C” shape that is found in literature (Shotyk, 1988), where the middle zone has low ash content, which increases above and below this zone. Given the low ash content in the SMDS core and the fact that the core was taken from the top of the dome of the ombrotrophic bog, the minerogenic material is concluded to be predominantly of aeolian origin. The source of the aeolian dust is yet unknown, but the ATR-FTIR and XRF-CS analyses of ashed peat can be used to characterize the material and relative changes in dust sources. However, to further interpret the source of the minerogenic material and the degree of aeolian reworking processes, grain size analysis and microscopic determination of roundness is recommended.

In the northern Store Mosse, Svensson (1988a) found *Carex* peat on the mineral soil followed by *Sphagnum* peat types that show varying degree of humification. The peatland development stages for Store Mosse are described by Kylander et al. (2013), Svensson (1988a) and Malmer et al. (1997) and include a fen stage which is followed by three bog stages. A full macrofossil analysis is required to clearly define stage boundaries, but significant decreases in bulk density values should imply the beginning of a new bog stage (Kylander et al., 2013). In the southern part of the bog, high-resolution peat accumulation rates showed very high values between 5500 and 4500 cal yr BP (Kylander et al., 2013). It has been hypothesised that this high peat accumulation event was generated by a shift in dust source, which increased nutrient input and productivity of the peatland ecosystem (Kylander et al., 2018). However, the SMDS core only covers the last 4800 years and thus only overlap with the last 300 years of the high peat accumulation event in the southern Store Mosse.

The basal peats of the SMDS core show higher ash content which reflects a more minerotrophic peat that has received more material during formation. The plants during a fen stage have abundant supply of nutrients and are richer in mineral matter. As peat accumulation continues with time, the subsequent plants have continuously lower availability to nutrients and the increased thickness of the peat limits external material to enter the mire (Shotyk, 1988). In the SMDS core, the organic bulk density and PAR show high values from the bottom and increase to peak at 4600 cal yr BP and thereafter start to decrease until ca. 4200 cal yr BP. The ash content follows a similar trend. This period is interpreted as changes in the hydrology and vegetation on the site of the SMDS core, which could result in a transition from fen to bog stage (Loisel et al., 2014). Henceforth, it is assumed that around 4200 cal yr BP marks the beginning of ombrotrophic conditions and the *Sphagnum* dominated stages in the bog development. From the macrofossil analysis by Svensson (1988a) it is discussed that the transition results in a *Sphagnum fuscum* dominated vegetation.

The most notable increase in bulk density and PAR values occur at 3590 cal yr BP and is followed by another increase at 3210 cal yr BP. The highly humified layer around 3500 cal yr BP (320 cm) is consistent with findings in Svensson (1988a) who reported a layer of humified peat at 3 m depth. Svensson (1988a) linked this humified layer to a distinct layer of *S. ericaceae* and *S. vaginatum* peat in the southern bog area. Since the bulk density values rapidly decrease already 110 years later, 3520 cal yr might also indicate a shift in bog development.

Around 2100 cal yr BP (204 cm), bulk density and PAR values decrease, suggesting a new shift in the bog development. This corresponds to a likely shift observed by Svensson (1988a) in the northern Store Mosse, where highly humified peat is replaced by slightly or moderately humified *Sphagnum* peat. This shift was also observed in the southern bog area

at 2145 and 2480 cal yr BP and is interpreted as a botanical shift in the bog from *Sphagnum fuscum* to the *Sphagnum rubellum/Sphagnum fuscum* stage (Kylander et al., 2013; Svensson, 1988a). Consequently, it can be hypothesised that the stage *S. rubellum/S. fuscum* begins around 2100 cal yr BP at the SMDS site.

From the evidence available from previous studies and new bulk density and PAR values, it is not clear when the next botanical shift occurs. Observations by Svensson (1988a) suggests that the topmost 2 meters of peat in northern Store Mosse consists of *Sphagnum* peat types, generally *S. magellanicum*. Using changepoint modelling, Kylander et al. (2013) suggested the boundary to the *Sphagnum magellanicum* stage at 1230 cal yr BP and earlier dating by Malmer et al. (1997) suggests a shift at 1000 cal yr BP. The trends for bulk density and PAR values are variable between 1500 and 600 cal yr BP and show two significant decreases as at 890 and 660 cal yr BP. In the southern bog area, the bulk densities show gradual changes between 1330 and 865 cal yr BP and thereafter remain low until increasing the last 200-250 years (Kylander et al., 2013). It is hypothesised that the two significant decreases in bulk density and PAR values in the SMDS core also display a shift in the bog development which is not present in the southern bog area.

The last 600 years predominantly show increasing bulk density and PAR values. This increasing trend is more pronounced compared to bulk densities from the southern deposit records (Kylander et al., 2013). The surface peat shows higher ash content as well, which is interpreted as increasing contribution of industrial dust from anthropogenic activities.

6.2 Spectral Signals from the Bulk Peat

All of the identified peaks from the factor loadings of the ATR-FTIR PCA for both bulk and ashed peat samples, together with the assigned molecular bond and the component(s) associated with the specific wavenumber(s) can be found in Appendix, Table 10. A summary of the interpretation for each principal component is displayed in Table 4.

BPC1 show high factor loadings for a substantial amount of absorption peaks. Wavenumbers 2918 and 2850 cm^{-1} are associated with the antisymmetric and symmetric CH_2 stretching vibrations of fats, wax and lipids (Cocozza et al., 2003; Niemeyer et al., 1992; Ning, 2011). If these bands are more prominent than 2960 and 2870 cm^{-1} , it suggests many CH_2 groups and few CH_3 groups in the sample (Ning, 2011). The spectral region 2500-2000 cm^{-1} shows high loadings and this region is characteristic of triple bonds and accumulated double bonds (Ning, 2011) and also for carboxylate ions (Krumins et al., 2012). BPC1 also has high factor loadings in the region 1736-1157 cm^{-1} , where lignin associated compounds and carboxylic acids have their main vibrations. For example, 1608 and 1512 cm^{-1} are indicative of aromatic C=C stretching vibrations in lignin and other aromatics (Cocozza et al., 2003; Niemeyer et al., 1992), 1466 and 1373 cm^{-1} are associated with C-H deformations in phenolic (lignin) and aliphatic structures or in the methyl group (Ning, 2011; Parker, 1971) and 1267 and 1228 cm^{-1} are associated with C-O stretching of phenolic OH (Ibarra et al., 1996; Niemeyer et al., 1992). In addition, 839 cm^{-1} can also be linked to the aromatic CH out-of-phase bending vibration in lignin (Niemeyer et al., 1992; Zaccheo 2002). High factor loadings are also shown for 1720 and 1705 cm^{-1} , assigned to C=O stretch of COOH/COOR in e.g. carboxylic acids, aldehydes and ketones (Cocozza et al., 2003; Gondar et al., 2005; Niemeyer et al., 1992). Finally, 719 cm^{-1} shows high factor loadings, and is associated with CH_2 wagging in alkanes with more than four CH_2 groups (Ning, 2011).

BPC1 shows negative loading for wavenumbers 3905-3633 cm^{-1} , indicative of OH-vibrations in hydroxyl groups (Ning, 2011), and for 1059 and 1032 cm^{-1} , where a combination of C-O stretching and O-H deformation is characteristic for the polysaccharide vibration

modes (Grube et al., 2006; Krumins et al., 2012). The factor scores (min. -2.16, max. 3.65) for BPC1 decrease from the bottom until ca. 4200 cal yr BP when they stabilize around average until ca. 2000 cal yr BP when they decrease further (Figure 5). BPC1 factor scores are moderately correlated with age ($n = 82$; $r = 0.67$).

Fresh *Sphagnum* consists predominantly of polysaccharides and is also rich in phenols (e.g. Sphagnum acid), but lacks lignin compounds completely (van Breemen, 1995). Increased peat humification is expected with depth, and it is therefore expected with a decline of the main polysaccharides markers and a relative increase in main lignin bands and aliphatic structures (Artz et al., 2008). Polysaccharides are more susceptible to degradation than aliphatic compounds or lignin, which will affect how these compounds are changing with depth (Kylander et al., 2018). The BPC1 factor scores show a very similar trend to bulk density and PAR, where high BPC1 scores coincides with high bulk density and PAR values. High factor loadings are seen for the C-H absorption bands, which are interpreted as aliphatic hydrocarbons and presence of methyl groups, compounds that are commonly developed during decomposition of peat (Krumins et al., 2012). The C-O absorption bands of polysaccharides have low loadings and can be associated with polymeric carbohydrates such as cellulose, that are broken apart during decomposition of peat. Decomposition also results in disintegration of carboxylic acid and carboxylate ions (C=O bonds), which are substituted by more stable and resistant compounds (Krumins et al., 2012). From these evidence, high factor scores for BPC1 can therefore be linked to high decomposition, which co-vary with high bulk density values, suggesting that the factor show gradual degradation of peat.

BPC2 shows factor loadings almost opposite of BPC1, except for lower wavenumbers (Figure 9). In comparison with BPC1, the factor scores are more variable with depth and do not show the strong correlation with age (Figure 5). If the factors loadings are compared to those of BPC1 (Figure 7), one can see that wavenumbers 3905-3633 and 2050 cm^{-1} have relatively high loadings and 895, 839 and 719 cm^{-1} have relatively low loadings on factor BPC2. The range of absorption peaks at 3905-3633 cm^{-1} is indicative of OH-vibrations in hydroxyl groups (Ning, 2011). The OH group is present in alcohols and in theory they do not show significant changes with peat age or depth (Krumins et al., 2012). OH-vibrations can also indicate presence of water or clays (Müller et al., 2014). Absorption at 2050 cm^{-1} also show high loadings, which lies in the region for triple bonds and carboxylate ions (Krumins et al., 2012; Ning, 2011). Highly negative factor loadings are seen for 895 cm^{-1} which is possibly related to vibrations of the last H in 5-substituted benzene ring (Ning, 2011) while 839 cm^{-1} is linked to aromatic CH out-of-phase bending in lignin (Niemeyer et al., 1992; Zaccheo et al., 2002). The variation absorptions bands related to lignin indicate a change in other plant compounds, since there is no lignin in *Sphagnum* mosses (van Breemen, 1995). Lignin are mostly found in cell walls and are characterized by phenolic (hydroxy-aromatic) structures and after cellulose, lignin covers most of the remaining material of wood. Higher plants contain around 15-25% lignin and 30-50% carbohydrates (mainly cellulose) (Killops & Killops, 2013). The band at 719 cm^{-1} also has negative loadings, and associated with absorption of CH_2 wagging in long chain alkanes (Larkin, 2011; Ning, 2011). From the loadings on the different bands, BPC2 is interpreted as changes in bog vegetation.

BPC3 have highly positive factor loadings for wavenumbers 719 and 559-420 cm^{-1} (Figure 9). 719 cm^{-1} is associated with CH_2 wagging in alkanes with more than four CH_2 groups. However, several inorganic compounds also show absorption peaks around 700 cm^{-1} . Absorption at 895 cm^{-1} is probably related to vibrations of the last H in 5-substituted benzene ring (Ning, 2011). The range of peaks between 559 and 420 cm^{-1} are commonly related to molecular vibrations of inorganic compounds such as TiO_2 (700-500 cm^{-1}) phosphate (650-

530 cm^{-1}), sulphate (670-560 cm^{-1}), silicate minerals (500-440 cm^{-1}). However, also aromatic ring bending frequencies (700-300 cm^{-1}) (Colthup et al., 1990). Moderately negative loadings are shown for 1059 and 1032 cm^{-1} , assigned to the vibration modes of polysaccharides and alcoholic compounds (Grube et al., 2006; Krumins et al., 2012), as well as for 1736 and 1720 cm^{-1} , associated with C=O stretching vibrations of e.g. carboxylic acids and/or aromatic esters (Cocozza et al., 2003; Gondar et al., 2005; Krumins et al., 2012; Niemeyer et al., 1992).

The factor scores for BPC3 are quite variable throughout the core (Figure 5) but are not correlated with inorganic factors or ash content, which rule against the inorganic compounds with absorption bands below 700 cm^{-1} . Therefore, the low wavenumbers are likely vibrations of aromatic compounds. Aromatic compounds and long chain alkanes are hydrocarbons and resistant to degradation, while polysaccharides easily decompose. Given the loadings of the different bands, this factor is considered to represent the relative increase of polysaccharides and acids (negative factor scores) and hydrocarbons (positive factor scores).

BPC4 show high factor loadings for wavenumbers 2918, 2850, 1736, 1720 and 1705 cm^{-1} (Figure 9). 2918 and 2850 cm^{-1} are associated with the antisymmetric and symmetric CH_2 stretching vibrations of fats, wax and lipids and indicative of more CH_2 groups than CH_3 groups (Cocozza et al., 2003; Niemeyer et al., 1992; Ning, 2011). 1736, 1720 and 1705 cm^{-1} are associated with C=O stretching of COOH or COOR that is present in acids, aldehydes and ketones (Cocozza et al., 2003; Gondar et al., 2005; Krumins et al., 2012; Niemeyer et al., 1992). Negative factor loadings are seen for 667 and 559 cm^{-1} , which can be associated mainly with inorganic compounds (Colthup et al., 1990). The factor scores for BPC4 have several distinct decreases at 4300, 4000 and 3555 cal yr BP (Figure 5). In summary, the high loadings on factor BPC4 indicate the presence of more CH_2 groups than CH_3 groups, acids, aldehydes, ketones and fats, waxes and lipids. BPC4 factor scores show several similarities with the OBD and PAR. Given the loadings on the different absorption bands, this factor is considered to represent acidity and lipids (high factor scores).

6.3 Spectral Signals from the Ashed Peat

APC1 have highly positive factor loadings for 1203, 1163, 1147, 1101, 677, 646, 611, 594 and 563 cm^{-1} . The Si-O bond have strong absorption for the asymmetrical stretching vibrations cm^{-1} . The feldspar group show vibrations in the ranges 1200-900, 800-700 and 650-375 cm^{-1} (Müller et al., 2014) and the negative absorption peaks listed above fall within these ranges. The Si-O asymmetrical stretching vibration show a peak round 1100 cm^{-1} and is characteristic for silicates and clays (Müller et al., 2014). Negative factor loadings are seen for absorption peaks at 876, 451, 436 and 420 cm^{-1} . 876 and the range 1500-1400 cm^{-1} are characteristic for the asymmetric stretch and for the out-of-plane bending vibration, respectively, of the carbonate ion in calcite and dolomite (Müller et al., 2014). 451, 436 and 420 cm^{-1} could be relates to several inorganic compounds, for example Si-O-Si deformation and Si-O asymmetrical bending vibration in silicates and clays (Müller et al., 2014), but are difficult to assign to any specific compound. However, APC1 is well correlated with ash content and XPC2 (Fe, Mn, Ca) and these three profiles all show an apparent shift around 4100-4200 cal year BP. The compounds with absorption peaks in APC1 seem to be related to mobile elements and the fen-bog transition. Weathering of surrounding granitic rocks could produce a range of products, including quartz, clay minerals and numerous elements in solution. APC1 is interpreted as weathering products of surrounding rocks vs carbonates.

APC2 has highly positive factor loadings for 1510, 1495, 1477, 1412 and 513 cm^{-1} . The wavenumbers 1500-1400 cm^{-1} are characteristic for the asymmetric stretch of the carbonate ion (Müller et al., 2014). Absorption at 513 cm^{-1} is assigned to the Si-O asymmetrical bending

vibrations in silicates and clays. Negative factor loadings for 993, 958, 798, 779, 714 and (677) cm^{-1} , which are all characteristic for Si-O stretching and bending vibrations in silicate minerals (Müller et al., 2014). Feldspars show vibrations in the ranges 1200-900, 800-700 and 650-375 cm^{-1} , but it is difficult to separate different minerals since their vibration modes greatly overlap (Müller et al., 2014). From these loadings on the different bands, factor APC2 is interpreted as a mixture between carbonates (positive loadings) and silicates, probably feldspars (negative loadings).

APC3 has positive factor loadings for 3691, 3678, 3653 cm^{-1} , which is assigned to stretching and bending vibrations of the inner -OH groups in clays (illite, montmorillonite and kaolinite) (Müller et al., 2014). Clay minerals usually show IR spectra with three main areas: inner surface -OH groups, Si-O vibrations and Si-O-M vibrations. Illite contains quartz and should show overlapping vibrations with quartz, but there are additional illite peaks at 3630, 828 and shoulder at 915 cm^{-1} . Illite, montmorillonite and kaolinite are not possible to distinguish between in complex mixtures and small amounts (Müller et al., 2014). Negative factor loadings occur at 876, 798, 779 and 714 cm^{-1} , which occur in the region of Si-O stretching and bending vibrations (Müller et al., 2014). APC3 is interpreted, from the loadings on bands described above, as the signal of clays (positive factor loadings) and silicates, probably quartz (negative factor loadings).

APC4 has positive factor loadings for 1078, 1032, 1014, 993 and 958 cm^{-1} . Quartz typically show a broad peak in this region with a maximum at 1080 cm^{-1} for the asymmetric stretching vibration of the Si-O groups, but also have high absorption for vibrations at 800-780 and 450 cm^{-1} (Müller et al., 2014), which does not show significant loadings for the factor. However, the asymmetrical stretching vibrations occur in the range 1080-1200 and can also indicate vibrations in feldspar (Matteson & Herron, 2003). The negative factor loadings are seen for absorption peaks at 646, 611, 563 and 513 cm^{-1} . Plagioclase and K-feldspar commonly show absorption for the O-Si(Al)-O bending vibrations at 646, 611 and 594 cm^{-1} as well as for the Si(Al)-O stretching vibrations at 1032, 1014, 993 and 958 cm^{-1} (Matteson & Herron, 2003). The vibrations at 513 cm^{-1} is related to the asymmetrical bending vibrations of the Si-O bond, which is present in both quartz, clays and feldspars (Müller et al., 2014). From the loadings on the different bands, factor APC4 is interpreted as the mixture between different feldspars.

6.4 Interpretation of Changes in Spectral Data Over Time

The spectral data show a complex behaviour in the SMDS core. The interpretation for each factor from the two PCA on ATR-FTIR analyses are summarized in Table 4. At the bottom of the peat deposit until approximately 4200 cal yr BP, a period interpreted as the fen stage, weathering products (APC1) and decomposition (BPC1) show high factor scores. There are also high factor scores for the acids and lipids (BPC4) until 4040 cal yr BP. BPC2 (vegetation change) show a shift from negative to positive factor scores around 4100 cal yr BP, which is expected when the peatland becomes ombrotrophic and favour plants that have affinity for poor nutrient conditions. During this time, BPC4 show high factor scores as well, indicating relatively high amounts of acids and lipids. BPC4 also show negative factor scores, indicative of higher amounts of acids and polysaccharides. APC3 and APC4 both show high negative factor scores between 4250 and 4000 cal yr BP, which suggest input of more clays. APC2 show positive factor scores between 4500 and 3500 cal yr BP and this suggest input of more carbonates than silicates (quartz).

Between 4000 and 2500 cal yr BP, APC1 predominantly show negative scores, indicating less weathering products and more carbonates. BPC1 and BPC2 continuously show positive

factor scores until 3100 cal yr BP, when they shift to negative. This suggests a bog development and vegetational shift occurring around 3100 cal yr BP. Around 4000 cal yr BP, BPC4 gradually shows more negative factor scores, indicating less lipids and acids. From 4000, APC3 and APC4 scores shift to positive, indicating input of more silicates (quartz) than clays and a change in feldspar input. APC2 show negative factor scores around 3500 cal yr BP, indicating more silicates than carbonates, but between 3400 and 2500 the factor scores shift to positive again.

Between 2500 and 1800 cal yr BP, BPC1 indicates increasing decomposition and thereafter the factor scores decrease. BPC2 shows large shifts in the vegetation between 2500 and 1250 cal yr BP, but the variations in the factor scores are linked to bulk density and PAR values. Around 2500 cal yr BP, BPC4 indicates a shift with increasing acids and lipid compounds while

BPC3 indicate increasing hydrocarbons (long chain alkenes and aromatics). APC1 factor scores remain negative, indicating more carbonates than weathering products, except for a peak around 2300 cal yr BP when weathering products increase. APC2 show another shift to negative scores around 2500 cal yr BP which suggests input of more silicates (quartz) than carbonates. The factors APC3 and APC4 both show rapidly decreasing factor scores around 2500 cal yr BP that can be interpreted as increasing clays and a shift in feldspars.

During the last 1250 years, BPC1 show negative factor scores and thus low decomposition, which is reasonable at the top of the peat profile. The vegetation factor (BPC2) rapidly change at 890 and 660 cal yr BP which coincides with rapid decreases in bulk density and PAR values as well as higher amounts of hydrocarbons (BPC3). BPC4 show continuously positive factor scores during the last 1250 years and this can be interpreted as high amounts of acids and lipids. APC1 predominantly show negative factor scores from 12500 until present and thus low amount of weathering products, but a peak around 500 cal yr BP indicates increasing weathering products. APC2 show mainly negative factor scores from 12500 cal yr BP but positive peaks at 1430, 1175, 840, 735 and 625-280 cal yr BP. APC3 indicates silicates (feldspar) at 1250-710 and 625-515 cal yr BP, and clays at 695-650 and 400-150 cal yr BP, where a significant negative peak is shown at 280 cal yr BP. Finally, APC4 indicate a shift in feldspars around 985, 665 and 385 cal yr BP.

6.5 Interpretation of Elemental Data

A summary of the interpretation of each principal component from the PCA on elemental data is shown in Table 5. The factor XPC1 show a similar behaviour for elements Zn, Cu, Pb, Si and Al which all are immobile in peat. The metals Zn, Cu and Pb are associated with

Table 4. Summary of factors from the PCA on ATR-FTIR data and their interpretation.

PCA	SMDS factors	Interpretation
FTIR bulk peat	BPC1	Decomposition
	BPC2	Changes in bog vegetation
	BPC3	Polysaccharides/acids vs hydrocarbons
	BPC4	Acids and lipids
FTIR ashed peat	APC1	Weathering products vs carbonates
	APC2	Carbonates vs silicates (feldspars)
	APC3	Clays vs silicates (quartz)
	APC4	Feldspar mixture

Table 5. Summary of factors from the PCA on XRF-CS data and their interpretation.

PCA	SMDS components	Interpretation
XRF-CS	XPC1	Anthropogenic dust
	XPC2	Mobile elements (fen-bog transition)
	XPC3	Coarse minerals
	XPC4	Source change

human mining since ancient times (Nriagu, 1998). This factor has high scores (Figure 11) for samples at the top of the profile (last 400 years). Concentrations of dissolved Pb in peatland surface waters is greatly influenced by closeness of anthropogenic sources (Shotyk, 1988), and the increase in XPC1 could result from increased mining (Nriagu, 1998). XPC1 is therefore interpreted as anthropogenic dust.

The factor XPC2 is associated with elements Ca, Mn and Fe which are mobile in the anoxic water table. For example, calcium is essential for plant growth and also reflects how much mineral soil water influence the peatland (Shotyk, 1988). XPC2 show a moderate correlation with depth that suggest that these elements are linked to decomposition of peat. Around 4000-3900 cal yr BP there is a transition from positive to negative scores, which is interpreted as the fen-bog transition of the peatland. Indeed, the factor scores show a similar trend to the inferred decomposition factor BPC1. XPC2 is interpreted to be associated with mobile elements and the fen-bog transition of the peatland.

The factor XPC3 is associated with Al, Si, Ti and Zr which are biogeochemically conservative elements. This component is interpreted as detrital input from atmospheric dust deposition, in excess of the anthropogenic dust deposition in factor XPC1. The shift in mineral dust composition around 5500-4500 cal yr BP in the southern bog area has been linked to increasing input of nutrients P, Ca and K to through a new dust source. The material is suggested to be more coarse and less weathered minerals (Kylander et al., 2018). Elemental data from southern Store Mosse suggested that the dust contain clays, mica, plagioclase feldspar, quartz, phosphate minerals, zircon and rutile (Kylander et al., 2016). Remarkably, the factor scores from XPC3 show an opposite trend to those of factor APC2. This implies, that an increase in XPC3 can be linked to increases in silicates, and possibly feldspars. A decrease in factor scores for XPC3 consequently implies an increase in carbonate minerals. From these arguments, factor XPC3 is interpreted as influx of weathered, coarse silicate minerals such as feldspars, where positive factor scores mean a high influx.

The factor XPC4 has high loadings for elements K and P. Both of these elements are limiting nutrients in the bog and an increased supply could enhance the productivity (Kylander et al., 2018). The factor scores for XPC4 show similarities to those of XPC3, suggesting that the two factors are related to each other. It is hypothesised that XPC4 show a source change of the dust.

6.6 Paleoclimatic Summary

Major shifts in bulk density and peat accumulation rates are compared to previous work at Store Mosse (Kylander et al., 2013, 2018; Svensson, 1988a) as well as other peatlands in southern Sweden (Rundgren, 2008) and southern Finland (Väliranta et al., 2007). The major trends of ash content, bulk density and PAR are put in a paleoclimatic perspective and compared to the timing of well-established regional events (Hass, 1996; Mayewski et al., 2004; Seppä et al., 2009). Finally, the variation in the spectral and elemental data are described over time, with implications for atmospheric dust influx and potential dust sources (Figure 12 and Figure 13).

The elemental data for factor XPC2 (Fe, Mn, Ca) show a rapid decrease in the factor scores around 4100 cal yr BP and shifts to negative scores around 3900 cal yr BP (Figure 13). The decrease of these redox sensitive elements indicates mineral-poor conditions with decreasing influence from ground water (Charman, 2002). This supports the earlier implication from bulk density and PAR values of a fen-bog transition around 4200 cal yr BP. From 4800 to around 4200 cal yr BP, there is a trend in the factor scores of BPC1 from highly decomposed material, towards increasing polysaccharides and less degradable material, which suggests less humified peat (Figure 13). During the fen stage, the spectral data also show decreasing amounts of acids and lipid components and increasing amounts of clays relative to silicates (quartz). *Sphagnum* tissues have high content of complex and recalcitrant compounds such as lipids, (Loisel et al., 2014), which rather would suggest an increase in these compounds with ombrotrophic bog conditions. However, there are some uncertainty regarding the low absorption wavenumbers ($>700\text{ cm}^{-1}$) in factor BPC3 and thus it is not clear if acids and lipids are indeed decreasing. It was suggested, that these wavenumbers also could reflect absorption from inorganic molecular vibrations. A transition towards more unstable climate in southern Sweden has been dated to 4600-3400 cal yr BP, with two significant stepwise shifts centred at 4400 and 3900 cal yr BP (Edvardsson et al., 2013). Around 4000 cal yr BP, low lake levels have been observed in central and southern Sweden,

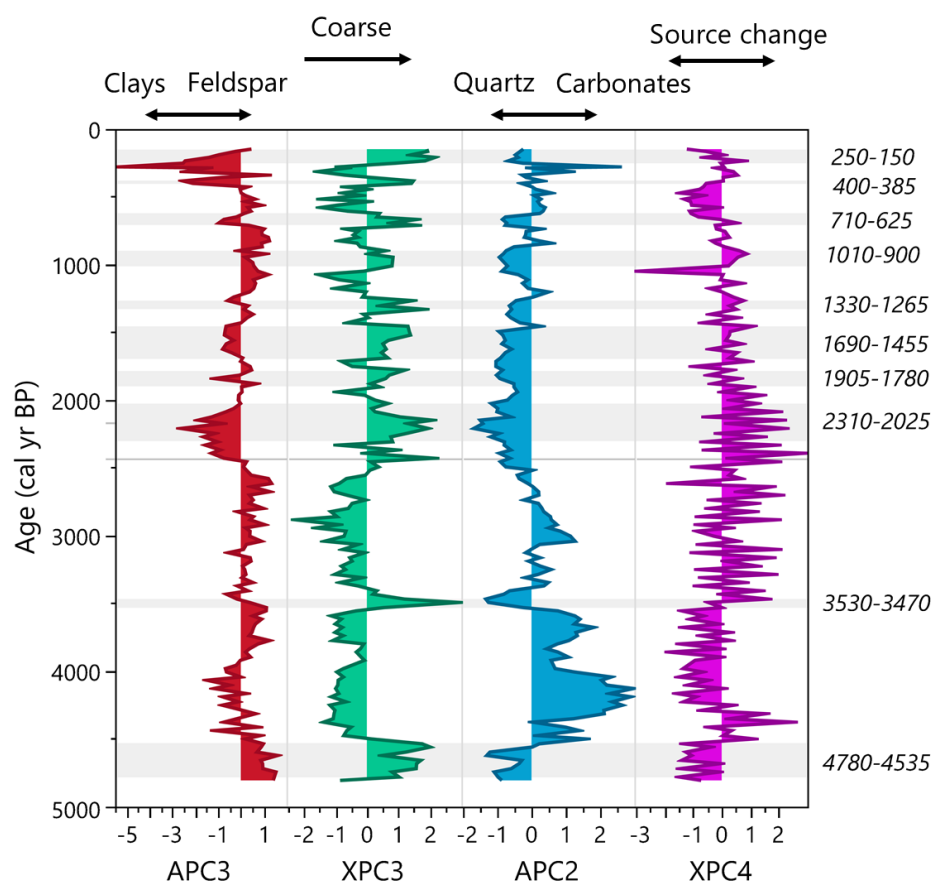


Figure 12. Interpretation of inorganic proxies for the SMDS core, including factor scores for APC2, APC3, XPC3 and XPC4. These proxies originate from the PCA on ATR-FTIR spectroscopic analyses of bulk and ashed peat samples. APC3 is used as a proxy for clays versus feldspars. XPC3 indicates influx of coarse-grained minerals. The black stars indicate peaks with high influx of coarse-grained minerals. These peaks coincide well with negative factor scores for factor APC2, which shows the relative amounts of quartz to carbonates. Finally, XPC4 shows a shift in dust source over centennial to millennial time.

suggesting a drier climate (Almquist-Jacobson, 1995; Edvardsson et al., 2013). This could affect the water table in Store Mosse as well, and a lowering of the water table has been described as one mechanism that promotes bog development (Hughes & Barber, 2003).

From 4800-4500, factor XPC3 and APC3 show high factor scores, indicating high influx of coarse-grained, less-weathered silicate minerals such as feldspar (Figure 12). Factor APC2 show low factor scores at this time, indicating more input of silicate minerals (mainly quartz), than carbonate minerals. This period coincides with the high peat accumulation event in southern Store Mosse, which showed increasing deposition of coarse-grained, P-rich minerals and feldspar between 5500 and 4500 cal yr BP (Kylander et al., 2018). Concentrations of phosphorus show high values at 4500-4200 cal yr BP, but potassium show low values during this period, see Appendix, Figure 18.

The decreasing bulk density and PAR values at 3590 and 3210 cal yr BP show changes in the bog development and possible, a stage shift to *Sphagnum rubellum/Sphagnum fuscum*. At the same time, the spectral data proposes decreasing peat decomposition and vegetation changes, which support the hypothesis of a stage shift (Figure 13). In south-central Sweden, increases of lake-levels in Lake Ljustjärnen are dated to 3200 cal yr BP, which suggests a response to wetter and colder conditions (Almquist-Jacobson, 1995). Temperature reconstructions from stacked pollen-records indeed show cold conditions between 4000 and

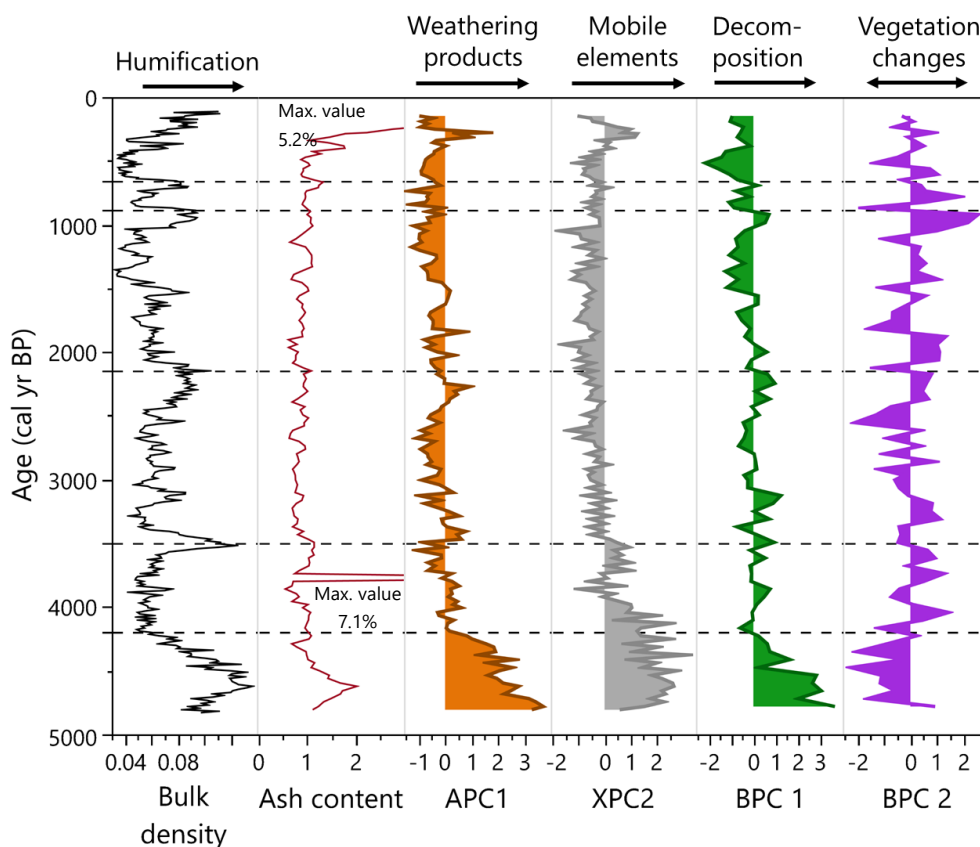


Figure 13. Interpretation of the proxies bulk density (g/cm^3), ash content (%) and factor scores APC1, BPC1 and BPC2. The factors originate from the PCA on ATR-FTIR spectroscopic data of bulk and ashed peat samples. Increasing bulk density is here used as a proxy for higher humification of the peat. APC2 show increasing amounts of weathering products with increasing factor scores. Factor XPC2 show higher amounts of the mobile elements below 4200 cal yr BP and indicates the fen-bog transition. Factor BPC1 indicate the degree of peat decomposition, where higher factor scores are linked to more decomposed peat. Finally, BPC2 indicates shifts in the bog vegetation.

3000 cal yr BP, with the lowest temperatures around 3500 cal yr BP (Seppä et al., 2009). Further, increased humification was reported from the bog surface wetness record from southern Finland between 3500 and 3200 cal yr BP (Väliranta et al., 2007). Compiled results from peat deposits in southern Sweden also show a shift to wetter conditions at this time, but their peak occur at 3300 cal yr BP (Rundgren, 2008).

Around 3500 cal yr BP, the spectral data from the SMDS core shows higher amounts of silicates (quartz) and feldspars relative to carbonates and clays (Figure 12). Factor XPC3 show a rapid shift to more coarse minerals as well. Interestingly, around 3500 cal yr BP factor XPC4 (K, P) suggest a source change of the dust deposited on the bog. Since the minerogenic material in the SMDS peat sequence is assumed to be essentially of aeolian origin, this implies that the mineral dust was transported from several alternating sources, local and/or regional. Further comparison with elemental data from surrounding bedrock and the sand dune system is needed to conclude if these sources has contributed to the atmospheric dust deposition at the SMDS site. However, in the northern hemisphere, a rapid climate change event with a cooling trend was dated to 3500-2500 cal yr BP, where strengthened westerlies over the North Atlantic and Siberia was observed from sea-wind proxies (Mayewski et al., 2004). Increasing wind strength could potentially activate aeolian deposits (Sorrel et al., 2012). In contrast, factor XPC3 shows a rapid shift towards less coarse material again around 3300 cal yr BP, suggesting that the input probably was derived during a shorter period of increased wind strength. It is possible, that an increasing storminess could be responsible, but this should show several peaks in the XPC3 factor scores. Stacked records of paleostorm activity in northern coastal Europe suggest a storm period starting a few hundred years later, at 3300-2400 cal yr BP (Sorrel et al., 2012), and increasing coarse minerogenic material was reported at 3675 cal yr BP in two other Swedish bogs (Hyltemossen and Boarps Mosse) in southernmost Sweden (Björck & Clemmensen, 2004).

Table 6. Peaks from XPC3 factor scores from the SMDS core compared to peaks in aeolian sand influx (quartz grains >2mm) in Hyltemossen (H) and Boarps Mosse (B) in southern Sweden (Björck & Clemmensen, 2004). The aeolian sand influx peak numbers are also displayed (3-10, 15 and 17).

SMDS peaks (cal yr BP)	Aeolian sand influx peaks from Björck and Clemmensen (2004) (cal yr BP)		
250-150	-	-	-
400-385	400	3a	H, B
710-625	700	4	H
1010-900	900	5a	H, B
	1000	5b	H
1330-1265	1350	6a	H
1690-1455	1450	6b	H, B
	1675	7	H, B
1905-1780	1800	8a	B
	1875	8b	H
2310-2025	2050	9b	H
	2150	10a	H, B
	2225	10b	H, B
	2300	10c	H
3530-3470	(3675)	(15)	(H)
4780-4535	4550	17	H

Despite the lack of a storm-signal in the SMDS core during the mid-Holocene, factor XPC3 and APC2 suggest increasing influx of coarse silicate minerals, mainly quartz during ten short periods around 2500 cal yr BP until the top of the peat sequence (Figure 12). Factor XPC4 indicate that there has not been any clear source change until around 1000 cal yr BP. 9 of these short but significant increases in coarse-grained silicate minerals coincides with influx of coarse-grained quartz in Hyltemossen and or Boarps Mosse (Björck & Clemmensen, 2004), and a comparison with their records is summarised in Table 6. The stacked paleostorm records suggests other period of increased storminess in northern Europe at 1900-1050, 600-250 cal yr BP and during the Little Ice Age (Sorrel et al., 2012). Although the climate variation during the late Holocene has shown large regional differences, there is

implications for increased storminess at this time (Kylander et al., 2018; Seppä et al., 2009). In the SMDS sequence, there are eight (perhaps nine) significant peaks during the late Holocene which suggest influx of more coarse-grained silicates and that can be linked to increased storminess in southern Sweden (Björck & Clemmensen, 2004) and coastal northern Europe (Sorrel et al., 2012) (Table 6).

Around 2100 cal yr BP (204 cm), bulk density and PAR values decrease, suggesting a shift in bog development. This corresponds with a likely shift observed by Svensson (1988a) in the northern Store Mosse, from highly humified peat to slightly or moderately humified *Sphagnum* peat. This shift was also observed in southern Store Mosse around at the same time and was interpreted as a botanical shift in the bog from *S. fuscum* to *S. rubellum*/*S. fuscum* (Kylander et al., 2013; Svensson, 1988a). At 2100 cal yr BP, the factor scores for BPC1 suggest slightly more decomposed material, but then the scores gradually decrease and shift to negative around 1900 cal yr BP, suggesting gradually less decomposed material in the peat sequence (Figure 13). Additionally, the factor scores for XPC2 show a gradual decrease in redox sensitive elements until ca. 1900 cal yr BP when the scores rapidly increase. Dry climatic conditions commonly produces a highly humified peat layer, while less humified peat deposits form during periods with increased bog wetness (Svensson, 1988a). Pollen-based reconstructions of mean annual temperature in northern Europe show a peak in temperatures at 2000 cal yr BP, which was consistent with dry conditions in the bog surface wetness record (Hass, 1996; Väiliranta et al., 2007). Around 2000 cal yr BP, a lowering of lake levels can be seen in pollen records from Lake Ljustjärnen in the county of Örebro (Almquist-Jacobson, 1995). If the dry conditions lowered the water table in northern Store Mosse, it would have required some time for the change to affect bog vegetation. It is likely that the highly humified layer indicate a warmer and drier climate, which decreases peat accumulation in the Store Mosse bog.

The climate during the last 1000 years is associated with a general cooling trend, but with large temperature oscillations (Hass, 1996). The trends for bulk density and PAR values in the SMDS core are increasing during this time, but also show with two significant decreases as at 890 and 660 cal yr BP. Around this time, the factor scores for BPC2 suggests major shifts in the bog vegetation (Figure 13). It is suggested that the northern bog area shows a varied vegetation development at this time, and due to peat cutting close to the site the surface peat sometimes show a more decomposed nature (Svensson, 1988a). The 890 cal yr decrease probably occur during the Medieval Warm Period, when temperatures were increasing in northern Europe (Hass, 1996; Seppä et al., 2009).

The last 600 years largely show increasing bulk density and PAR values, indicating wetter and/or colder conditions in the bog. This cold anomaly is more pronounced compared to the previously studied southern site in Store Mosse (Kylander et al., 2013). Mean annual temperature reconstructions from pollen records show a cold anomaly between 500 and 100 cal yr BP (Seppä et al., 2009). Further, the pollen-based record from Lake Ljustjärnen show increasing lake-levels around 300 cal yr BP (Almquist-Jacobson, 1995). This period is commonly referred to as the Little Ice Age. The surface peat shows low decomposition from the factor scores of BPC1, which is expected as the surface peat consists of fresh *Sphagnum* species. Around 500 cal yr BP, the spectral data shows a rapid change to more carbonate minerals (APC2) and more clays (APC3) (Figure 12). Higher ash content and increasing factor scores for APC4 and XPC1 are seen in the surface peat as well, which is interpreted as increasing contribution of anthropogenic dust and less-weathered minerals deposited on the bog surface (Figure 6 and Figure 10).

7 Conclusions and Future Prospects

The major advantage of FTIR compared to conventional methods is the possibility to extract information on both organic and organic components in peat. Since FTIR is fast and requires no or little sample preparation, this is useful for an overview of the peat profile before including several analytical techniques. PCA was performed on the spectral data set, which enabled the extraction of different components of the spectra, and consequently the factor scores allowed for analyses of these components over time. 4800 years of paleoclimatic history from the northern Store Mosse has been made, unfolding a complex bog development which at times diverges from that in the southern bog area. Although few radiocarbon dates were made on the lower parts of the SMDS peat sequence, it can be assumed that the overall peat accumulation trend is captured during the last 2000 years.

Analysis of the bulk density, PAR and ash content suggests an initial fen stage until 4200 cal yr. The fen-bog transition is further supported by shifts in decomposition (BPC₁), bog vegetation (BPC₂), mobile elements (XPC₂). Thereafter, at least three bog stages are suggested. At 3500 cal yr BP, the elemental data suggests a source change in the atmospheric dust deposition, possibly linked to increasing westerlies over the North Atlantic. Increased dust influx was however not seen until 2500 cal yr BP, when the spectral and elemental data show ten periods of rapid increases in coarse-grained silicate minerals. At least eight of these periods coincide with aeolian sand influx in the southernmost Sweden and can be correlated to periods of increased storminess over northern coastal Europe. The last 1000 years show a variable bog development with several shifts in bog vegetation and humification. The surface peat is characterized by less decomposed peat and large amounts of anthropogenically derived dust, as well as increasing amounts of clays and carbonate minerals.

To more clearly determine the different stage boundaries of the peat development in the northern Store Mosse, a full macrofossil analysis is required. This could provide a better understanding for the vegetational development of the peatland. Given the few radiocarbon dates for the SMDS peat core and the fact that a high peat accumulation event has been observed in the southern bog area, the age-depth model has considerable uncertainty for the lower peat sequence. Additionally, grain size analysis and/or microscopic analysis of the roundness of individual grains could produce more robust evidence of the variation in mineral dust sources and implications on the transport distance from the source. Finally, conventional XRD analyses could be used for comparison with the ATR-FTIR data and to further test the accuracy of this method. This could also help in the identification of certain minerals that show overlapping absorption peaks with the ATR-FTIR method.

8 Acknowledgements

I would like to thank my supervisor Malin Kylander for your dedication and help with this project and for introduction to peatlands and the methodology. Also, many thanks for being a part of a fantastic team where Malin Kylander, Jenny Sjöström, Eleonor Ryberg, Austin Stout and Teresa Olsson are thanked for sampling of the peat core. Thank you, Carina Johansson for great help during freeze-drying and lab-work. Voula Mylona is also thanked for ashing of additional samples as part of her practical course. Antonio Martínez Cortizas is much appreciated for all help with FTIR and interpretation of spectra and Noemi Alvarez Fernández is thanked for help with the R script and support with running it. Many thanks to the rest of the Santiago crew for fantastic company: Olalla López Costas, Tim Mighall, Sofia Nannes, Richard Bindler and Colin Cooke. Finally, I want to thank my family and friends for the immense support I have received through this project and who is always there for me.

9 References

- Abigail Matteson, Michael M. Herron. (2003). End-Member Feldspar Concentrations Determined by FTIR Spectral Analysis. *SEPM Journal of Sedimentary Research*, Vol. 63(6), 0–4. <https://doi.org/10.1306/d4267cc6-2b26-11d7-8648000102c1865d>
- Almquist-Jacobson, H. (1995). Lake-level fluctuations at Ljustjärnen, central Sweden and their implications for the Holocene climate of Scandinavia. *Palaeogeography, Palaeoclimatology, Palaeoecology*, 118(3–4), 269–290. [https://doi.org/10.1016/0031-0182\(95\)00002-2](https://doi.org/10.1016/0031-0182(95)00002-2)
- Álvarez-Fernández, N., & Martínez-Cortizas, A. (2019). SDP package for R. Universidade de Santiago de Compostela: Earth System Science Group.
- Artz, R. R. E., Chapman, S. J., Jean Robertson, A. H., Potts, J. M., Laggoun-Défarge, F., Gogo, S., ... Francez, A. J. (2008). FTIR spectroscopy can be used as a screening tool for organic matter quality in regenerating cutover peatlands. *Soil Biology and Biochemistry*, 40(2), 515–527. <https://doi.org/10.1016/j.soilbio.2007.09.019>
- Björck, S., & Clemmensen, L. B. (2004). Aeolian sediment in raised bog deposits, Halland, SW Sweden: A new proxy record of Holocene winter storminess variation in southern Scandinavia? *Holocene*, 14(5), 677–688. <https://doi.org/10.1191/0959683604hl746rp>
- Blaauw, M., & Christeny, J. A. (2011). Flexible paleoclimate age-depth models using an autoregressive gamma process. *Bayesian Analysis*, 6(3), 457–474. <https://doi.org/10.1214/11-BA618>
- Bond, G., Showers, W., Cheseby, M., Lotti, R., Almasi, P., DeMenocal, P., ... Bonani, G. (1997). A pervasive millennial-scale cycle in North Atlantic Holocene and glacial climates. *Science*, 278(5341), 1257–1266. <https://doi.org/10.1126/science.278.5341.1257>
- Bruker. (2019). XRF Data Differences: Quantitative, Semi-Quantitative, and Qualitative Data. Retrieved April 5, 2019, from <https://www.bruker.com/products/x-ray-diffraction-and-elemental-analysis/handheld-xrf/xrf-data-primer-quantitative-semi-quantitative-qualitative.html>
- Charman, D. (2002). *Peatlands and Environmental Change*. John Wiley & Sons Ltd.
- Chesworth, W., Cortizas, A. M., & García-Rodeja, E. (2006). Chapter 8 The redox-pH approach to the geochemistry of the Earth's land surface, with application to peatlands. *Developments in Earth Surface Processes*, 9(C), 175–195. [https://doi.org/10.1016/S0928-2025\(06\)09008-0](https://doi.org/10.1016/S0928-2025(06)09008-0)
- Cocozza, C., D'Orazio, V., Miano, T. M., & Shoty, W. (2003). Characterization of solid and aqueous phases of a peat bog profile using molecular fluorescence spectroscopy, ESR and FT-IR, and comparison with physical properties. *Organic Geochemistry*, 34(1), 49–60. [https://doi.org/10.1016/S0146-6380\(02\)00208-5](https://doi.org/10.1016/S0146-6380(02)00208-5)
- Colthup, N. B., Daly, L. H., & Wiberley, S. E. (1990). MAJOR SPECTRA-STRUCTURE CORRELATIONS BY SPECTRAL REGIONS. In *Introduction to Infrared and Raman Spectroscopy* (3rd ed., pp. 387–481). Elsevier. <https://doi.org/10.1016/B978-0-08-091740-5.50016-8>
- Edvardsson, J., Leuschner, H. H., Linderson, H., Linderholm, H. W., & Hammarlund, D. (2013). South Swedish bog pines as indicators of Mid-Holocene climate variability. *Lundqua Thesis*, 30(68), 93–103. <https://doi.org/10.1016/j.dendro.2011.02.003>
- Franzén, L. G. (2006). Chapter 11 Mineral matter, major elements, and trace elements in raised bog peat: a case study from southern Sweden, Ireland and Tierra del Fuego, south Argentina. In I. P. Martini, A. Martínez Cortizas, & W. Chesworth (Eds.), *Peatlands: Evolution and Records of Environmental and Climate Change* (1st ed., Vol. 9, pp. 241–269). Elsevier Science. [https://doi.org/10.1016/S0928-2025\(06\)09011-0](https://doi.org/10.1016/S0928-2025(06)09011-0)
- Gondar, D., Lopez, R., Fiol, S., Antelo, J. M., & Arce, F. (2005). Characterization and acid-base properties of fulvic and humic acids isolated from two horizons of an ombrotrophic peat bog. *Geoderma*, 126(3–4), 367–374. <https://doi.org/10.1016/j.geoderma.2004.10.006>
- Grube, M., Lin, J. G., Lee, P. H., & Kokorevicha, S. (2006). Evaluation of sewage sludge-based compost by FT-IR spectroscopy. *Geoderma*, 130(3–4), 324–333. <https://doi.org/10.1016/j.geoderma.2005.02.005>
- Hass, H. C. (1996). Northern Europe climate variations during late Holocene: Evidence from marine Skagerrak. *Palaeogeography, Palaeoclimatology, Palaeoecology*, 123(1–4), 121–145. [https://doi.org/10.1016/0031-0182\(95\)00114-X](https://doi.org/10.1016/0031-0182(95)00114-X)
- Hughes, P. D. M., & Barber, K. E. (2003). Mire development across the fen-bog transition on the Teifi floodplain at Tregaron Bog, Ceredigion, Wales, and a comparison with 13 other raised bogs. *Journal of Ecology*, 91(2), 253–264. <https://doi.org/10.1046/j.1365-2745.2003.00762.x>
- Ibarra, J. V., Muñoz, E., & Moliner, R. (1996). FTIR study of the evolution of coal structure during the coalification process. *Organic Geochemistry*, 24(6–7), 725–735. [https://doi.org/10.1016/0146-6380\(96\)00063-0](https://doi.org/10.1016/0146-6380(96)00063-0)
- Khoshhesab, Z. M. (2012). Reflectance IR Spectroscopy. In T. Theophile (Ed.), *Infrared Spectroscopy -*

- Materials Science, Engineering and Technology* (pp. 233–244). InTech.
<https://doi.org/10.5772/37180>
- Killops, S., & Killops, V. (2013). Chemical Composition of Organic Matter. In *Introduction to Organic Geochemistry* (2nd ed., pp. 30–70). Malden, MA USA: Blackwell Publishing Ltd.
<https://doi.org/10.1002/9781118697214.ch2>
- Krumins, J., Klavins, M., Seglins, V., & Kaup, E. (2012). Comparative Study of Peat Composition by using FT-IR Spectroscopy. *Material Science and Applied Chemistry*, 26, 106–114. Retrieved from
<https://ortus.rtu.lv/science/en/publications/15301/fulltext>
- Kylander, M. E., Bindler, R., Cortizas, A. M., Gallagher, K., Mörth, C. M., & Rauch, S. (2013). A novel geochemical approach to paleorecords of dust deposition and effective humidity: 8500 years of peat accumulation at Store Mosse (the “Great Bog”), Sweden. *Quaternary Science Reviews*, 69, 69–82.
<https://doi.org/10.1016/j.quascirev.2013.02.010>
- Kylander, M. E., Martínez-Cortizas, A., Bindler, R., Greenwood, S. L., Mörth, C. M., & Rauch, S. (2016). Potentials and problems of building detailed dust records using peat archives: An example from Store Mosse (the “Great Bog”), Sweden. *Geochimica et Cosmochimica Acta*, 190, 156–174.
<https://doi.org/10.1016/j.gca.2016.06.028>
- Kylander, M. E., Martínez-Cortizas, A., Bindler, R., Kaal, J., Sjöström, J. K., Hansson, S. V., ... Rauch, S. (2018). Mineral dust as a driver of carbon accumulation in northern latitudes. *Scientific Reports*, 8(1), 1–10.
<https://doi.org/10.1038/s41598-018-25162-9>
- Lantmäteriet ©. (2019). Geodata Extraction Tool (GET). Retrieved from <https://maps.slu.se/>
- Larkin, P. J. (2011). *Infrared and Raman Spectroscopy - Principles and Spectral Interpretation*. *Infrared and Raman Spectroscopy*. Elsevier. <https://doi.org/10.1016/C2010-0-68479-3>
- Loisel, J., Yu, Z., Beilman, D. W., Camill, P., Alm, J., Amesbury, M. J., ... Zhou, W. (2014). A database and synthesis of northern peatland soil properties and Holocene carbon and nitrogen accumulation. *Holocene*, 24(9), 1028–1042. <https://doi.org/10.1177/0959683614538073>
- Malmer, N., Svensson, G., & Wallen, B. (1997). Mass balance and nitrogen accumulation in hummocks on a South Swedish bog during the late Holocene. *Ecography*, 20(6), 535–549.
<https://doi.org/10.1111/j.1600-0587.1997.tb00422.x>
- Mayewski, P. A., Rohling, E. E., Stager, J. C., Karlén, W., Maasch, K. A., Meecker, L. D., ... Steig, E. J. (2004). Holocene climate variability. *Quaternary Research*, 62(3), 243–255.
<https://doi.org/10.1016/j.yqres.2004.07.001>
- Müller, C. M., Pejčic, B., Esteban, L., Piane, C. D., Raven, M., & Mizaikoff, B. (2014). Infrared attenuated total reflectance spectroscopy: An innovative strategy for analyzing mineral components in energy relevant systems. *Scientific Reports*, 4, 1–11. <https://doi.org/10.1038/srep06764>
- Niemeyer, J., Chen, Y., & Bollag, J. M. (1992). Characterization of Humic Acids, Composts, and Peat by Diffuse Reflectance Fourier-Transform Infrared Spectroscopy. *Soil Science Society of America Journal*, 56(1), 135–140. <https://doi.org/10.2136/sssaj1992.03615995005600010021x>
- Ning, Y.-C. (2011). *Interpretation of Organic Spectra*. *Journal of Chemical Education* (1st ed., Vol. 49). Singapore: John Wiley & Sons (Asia) Pte Ltd. <https://doi.org/10.1002/9780470825181>
- Nriagu, J. O. (1998). Tales Told in Lead. *Science*, 281(5383), 1622–1623.
<https://doi.org/10.1126/science.281.5383.1622>
- Olsen, J., Anderson, N. J., & Knudsen, M. F. (2012). Variability of the North Atlantic Oscillation over the past 5,200 years. *Nature Geoscience*, 5(11), 808–812. <https://doi.org/10.1038/ngeo1589>
- Orme, L. C., Reinhardt, L., Jones, R. T., Charman, D. J., Barkwith, A., & Ellis, M. A. (2016). Aeolian sediment reconstructions from the Scottish Outer Hebrides: Late Holocene storminess and the role of the North Atlantic Oscillation. *Quaternary Science Reviews*, 132, 15–25.
<https://doi.org/10.1016/j.quascirev.2015.10.045>
- Parker, F. S. (1971). *Applications of Infrared Spectroscopy in Biochemistry, Biology, and Medicine*. Boston, MA: Springer US. <https://doi.org/10.1007/978-1-4684-1872-9>
- R Core Team. (2013). R: A language and environment for statistical computing. Vienna, Austria: R Foundation for Statistical Computing. Retrieved from <http://www.r-project.org/>
- Reimer, P. J., Edouard Bard, B., Alex Bayliss, B., Warren Beck, B. J., Paul Blackwell, B. G., & Christopher Bronk Ramsey, B. (2013). IntCal13 and Marine13 radiocarbon age calibration curves 0–50,000 years cal bp. *Radiocarbon*, 55(4), 1869–1887.
- Rundgren, M. (2008). Stratigraphy of peatlands in central and northern Sweden: Evidence of Holocene climatic change and peat accumulation. *Gff*, 130(2), 95–107.
<https://doi.org/10.1080/11035890801302095>
- Saikia, B. J., Parthasarathy, G., & Sarmah, N. C. (2008). Fourier transform infrared spectroscopic estimation of crystallinity in SiO₂ based rocks. *Bulletin of Materials Science*, 31(5), 775–779.

- <https://doi.org/10.1007/s12034-008-0123-0>
- SAS Institute Inc. (2019). JMP®. Cary, NC: SAS Institute Inc.
- Seppä, H., Bjune, A. E., Telford, R. J., Birks, H. J. B., & Veski, S. (2009). Last nine-thousand years of temperature variability in Northern Europe. *Climate of the Past*, 5(3), 523–535. <https://doi.org/10.5194/cp-5-523-2009>
- Shotyk, W. (1988). Review of the inorganic geochemistry of peats and peatland waters. *Earth Science Reviews*, 25(2), 95–176. [https://doi.org/10.1016/0012-8252\(88\)90067-0](https://doi.org/10.1016/0012-8252(88)90067-0)
- Sjöström, J. K. (2018). *Reconstruction of Holocene atmospheric mineral dust deposition from raised peat bogs in south-central Sweden (Licentiate thesis)*. Stockholm University.
- Sjöström, J. K., Bindler, R., Granberg, T., & Kylander, M. E. (2018). Procedure for Organic Matter Removal from Peat Samples for XRD Mineral Analysis. *Wetlands*. <https://doi.org/10.1007/s13157-018-1093-7>
- Sorrel, P., Debret, M., Billeaud, I., Jaccard, S. L., McManus, J. F., & Tessier, B. (2012). Persistent non-solar forcing of Holocene storm dynamics in coastal sedimentary archives. *Nature Geoscience*, 5(12), 892–896. <https://doi.org/10.1038/ngeo1619>
- Svensson, G. (1988a). Bog development and environmental conditions as shown by the stratigraphy of Store Mosse mire in southern Sweden. *Boreas*, 17(1), 89–111. <https://doi.org/10.1111/j.1502-3885.1988.tb00126.x>
- Svensson, G. (1988b). Fossil Plant Communities and Regeneration Patterns on a Raised Bog in South Sweden. *The Journal of Ecology*, 76(1), 41. <https://doi.org/10.2307/2260453>
- Väliranta, M., Korhola, A., Seppä, H., Tuittila, E. S., Sarmaja-Korjonen, K., Laine, J., & Alm, J. (2007). High-resolution reconstruction of wetness dynamics in a southern boreal raised bog, Finland, during the late Holocene: A quantitative approach. *Holocene*, 17(8), 1093–1107. <https://doi.org/10.1177/0959683607082550>
- van Breemen, N. (1995). How Sphagnum bogs down other plants. *Trends in Ecology & Evolution*, 10(7), 270–275. [https://doi.org/10.1016/0169-5347\(95\)90007-1](https://doi.org/10.1016/0169-5347(95)90007-1)
- Weiss, N. A. (2013). *Introductory Statistics* (9th ed.). Pearson.
- Wieder, R. K., & Vitt, D. H. (Eds.). (2006). *Boreal Peatland Ecosystems* (Vol. 188). Berlin, Heidelberg: Springer-Verlag Berlin Heidelberg. <https://doi.org/10.1007/978-3-540-31913-9>
- Zaccheo, P., Cabassi, G., Ricca, G., & Crippa, L. (2002). Decomposition of organic residues in soil: Experimental technique and spectroscopic approach. *Organic Geochemistry*, 33(3), 327–345. [https://doi.org/10.1016/S0146-6380\(01\)00164-4](https://doi.org/10.1016/S0146-6380(01)00164-4)

10 Appendix

10.1 Photos of the Fresh SMDS Core Sections



Figure 14. Images of fresh core sections of the SMDS core taken from two alternating holes. From the top the sections cover deposit depths C1) 20-120 cm, C2) 50-150 cm, C3) 125-225 cm, C4) 200-300 cm, C5) 275-375 cm and C6) 350-450 cm.

10.2 Specifications for the ATR device

Table 7. Specifications for the iS7 ATR device with a diamond prism.

Depth of penetration (d_p)	2.01 μm at 1000 cm^{-1}
Spectral range	25000-200 cm^{-1} , reduced signal 2500-1900 cm^{-1}
Refractive index	2.4 (at 500 nm)
Hardness	7000 Knoop or 10 on Mohs scale

10.3 Freeze-drier and Pump

Table 8. Freeze-drier and pump specifications.

Freeze-drier Coolsafe 55-4 Pro		Pump Leybold TRIVAC D8B	
Temperature cold trap	-55 °C	Pump capacity	8 m ³ /h
Total capacity	3 kg (total volume 4 kg)	Reseller	Low2High Vacuum AB
Manufacturer	LaboGene Ap-5, Denmark	Install date	2011-05-26
Reseller	LAB360° AB		
Install date	2013-09-25		

10.4 Age-depth Model

Table 9. The settings for the age-depth model produced with the Bacon package in R. The model was produced on April 12, 2019 and obtained accumulation rates (years per cm) estimated by Markov Chain Monte Carlo (MCMC) iterations for any age of the SMDS core.

Setting description	Setting	Value used
Minimum depth	#d.min	0
Maximum depth	#d.max	426
Depth interval	#d.by	1
Mean of gamma distribution	#acc.mean	10
Shape of gamma distribution	#acc.shape	1.5
Memory mean	#mem.mean	0.7
Memory strength	#mem.strength	4
Depths of any hiatuses	#hiatus.depths	NA
Mean of gamma distribution describing hiatus length	#hiatus.mean	1000
Shape of gamma distribution describing hiatus length	#hiatus.shape	1
Time scale (0=cal yr BP and 1= BC/AD)	#BCAD	0
Calibration curve (where 1=IntCal13, 2=Marine13, 3=SHCal13 and 4=ConstCal)	#cc	1
For cores with post-bomb dates (negative ^{14}C ages) where default is 0	#postbomb	0
Depth unit	#unit	cm
Distribution of dates (0=student-t distribution)	#normal	0
Distribution parameter a	#t.a	3
Distribution parameter b	#t.b	4
Core-wide age offset (default 0)	#d.R	0
Core-wide age offset standard deviation (default 0)	#d.STD	0
Probability in %	#prob	0.95

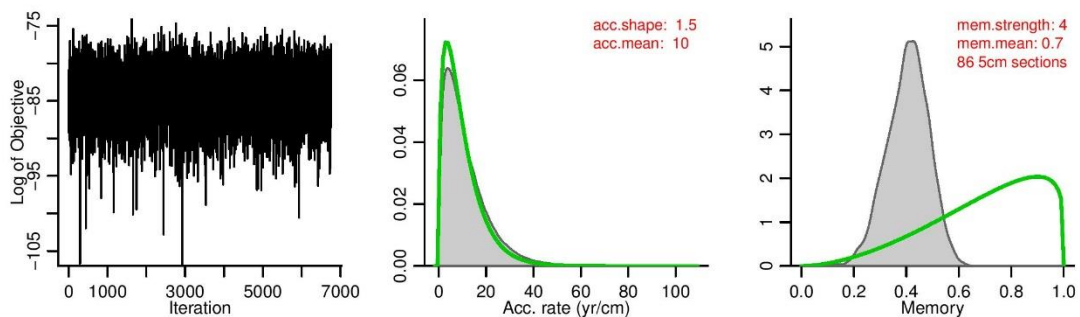


Figure 15. Bacon output graphical information, in addition to the age-depth model on the SMDS core. The panels show the MCMC iterations, the prior (green curves) and posterior (grey histograms) distributions for the accumulation rate (middle panel) and memory (right panel).

10.5 Selection of Absorption Peaks

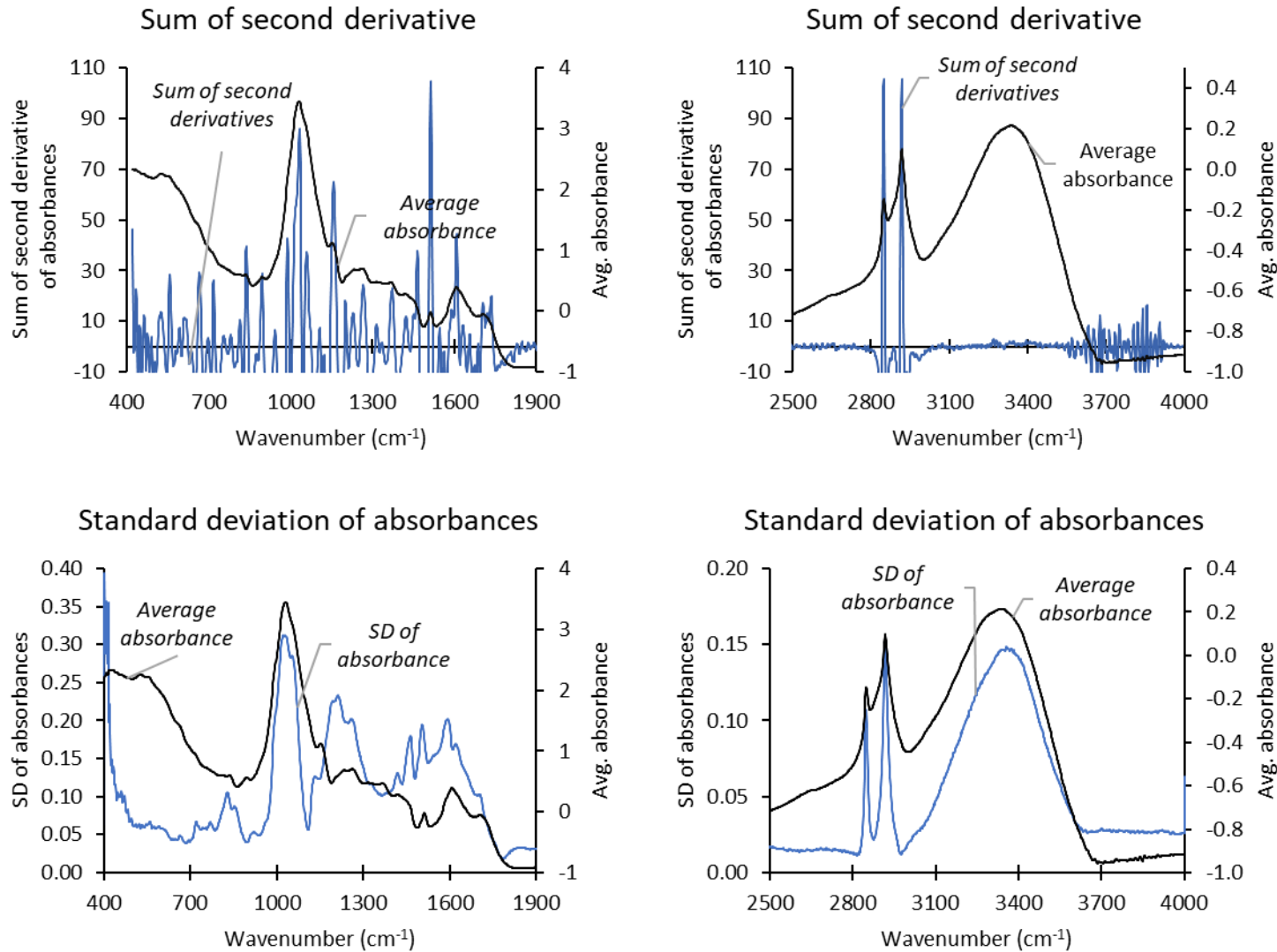


Figure 16. Data used in peak analysis on the ATR-FTIR data of bulk peat samples. The upper two graphs show the average absorbance and the sum of second derivatives of absorbance for wavenumbers 1900-400 cm⁻¹ (upper left) and 4000-2500 cm⁻¹ (upper right). The bottom two graphs show the average absorbance with standard deviation of absorbances for wavenumbers 1900-400 cm⁻¹ (bottom left) and 4000-2500 cm⁻¹ (bottom right).

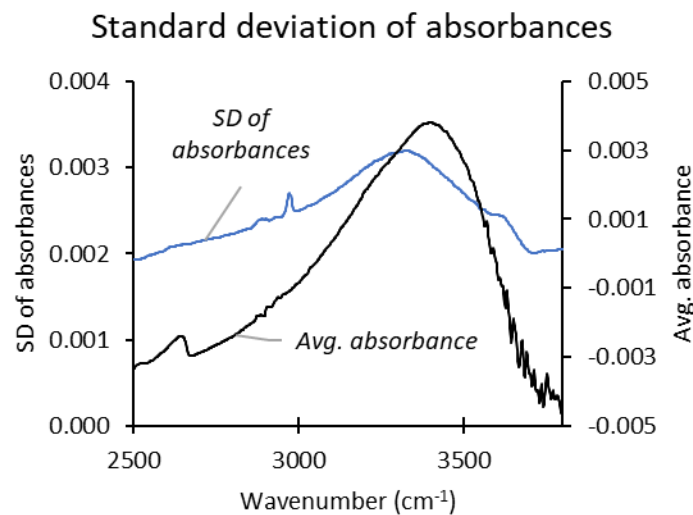
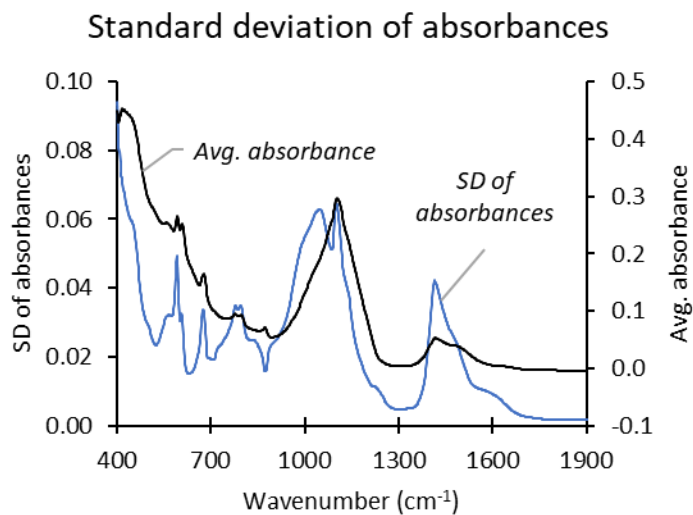
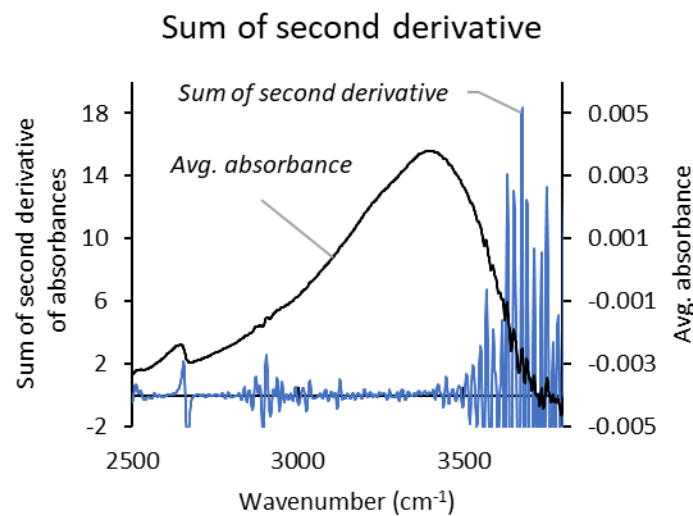
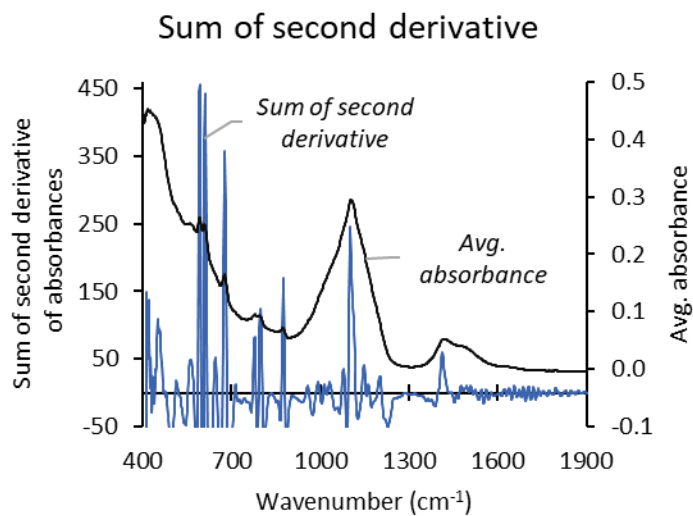


Figure 17. Data used in peak selection for principal component analysis on the ATR-FTIR data of ashed peat samples. The upper two graphs show the average absorbance and the sum of second derivatives of absorbance for wavenumbers 1900-400 cm⁻¹ (upper left) and 4000-2500 cm⁻¹ (upper right). The bottom two graphs show the average absorbance with standard deviation of absorbances for wavenumbers 1900-400 cm⁻¹ (bottom left) and 4000-2500 cm⁻¹ (bottom right).

10.6 XRF-CS Elemental Data Profiles

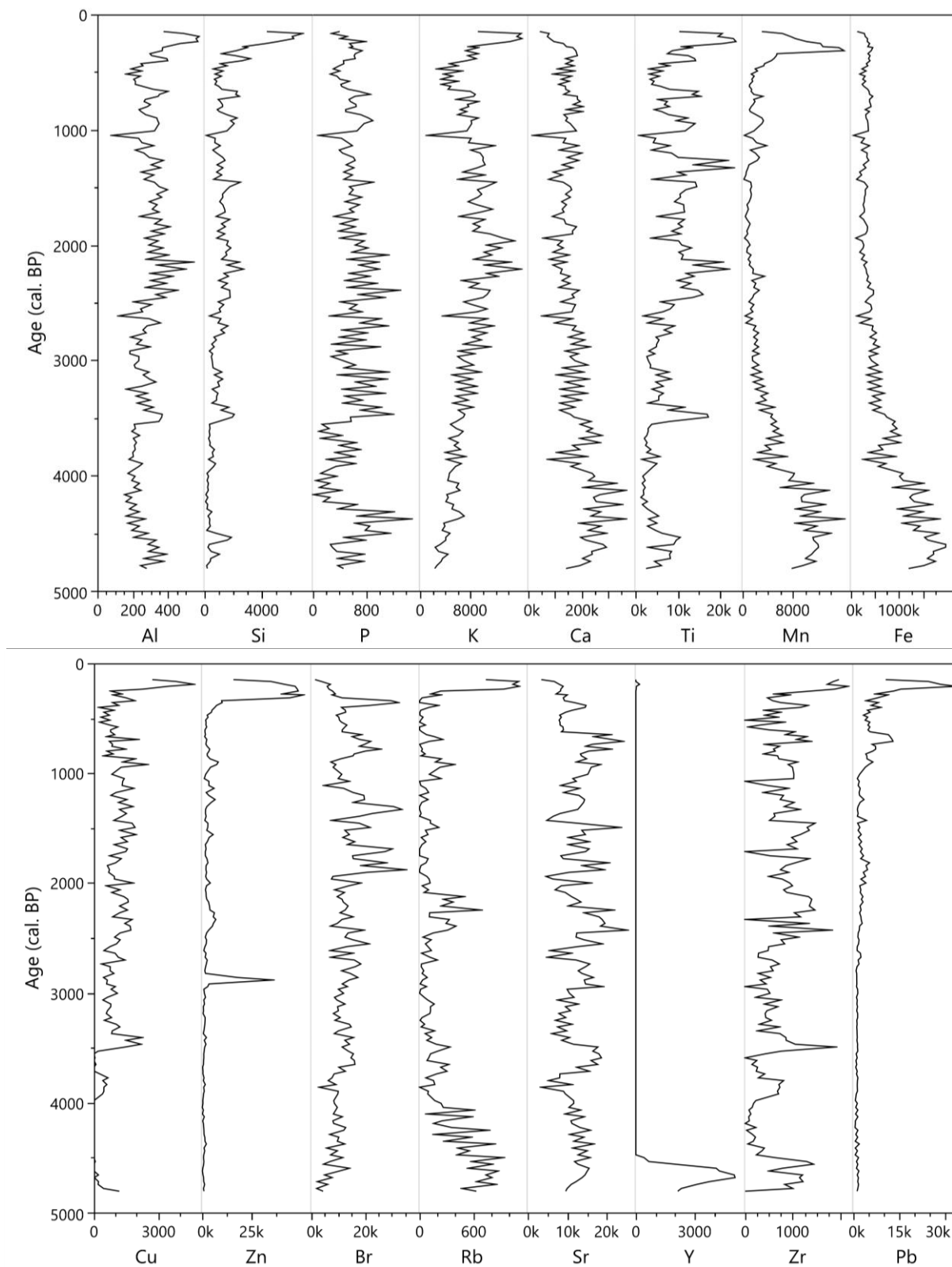


Figure 18. Elemental data from XRF-CS on ashed peat samples. The upper part shows elements Al, Si, P, K, Ca, Ti, Mn and Fe while the lower part shows Cu, Zn, Br, Rb, Sr, Y, Zr and Pb. All data is expressed as peak areas.

10.7 Interpretation of ATF-FTIR Wavenumbers

Table 10. Interpretation of identified wavenumber peaks from ATR-FTIR analyses on the SMDS bulk and ashed peat samples. The peaks are interpreted from their factor loadings from the PCA and are presented together with the assigned molecular bond and the component(s) associated with the specific wavenumber(s).

PC	Wavenumber (cm ⁻¹)	Peak assignment	Characterization / associated component	Reference
BPC1 BPC2	3900-3700	OH vibrations	Isolated hydroxyl groups	(Ning, 2011)
BPC1 BPC2 APC3	3700-3600	Stretching and bending vibrations of the inner surface -OH groups	Clays	(Krumins et al., 2012; Müller et al., 2014; Ning, 2011)
BPC1 BPC2 BPC3 BPC4	2918, 2850	Antisymmetric & symmetric CH ₂ stretching	Fats, waxes (lipids) with CH ₂ > CH ₃ groups	(Cocozza et al., 2003; Niemeyer et al., 1992; Ning, 2011)
BPC1 BPC2	2345, 2322	C-O	CO ₂ background error	(Ning, 2011)
BPC1 BPC2 BPC3	2500-1850 (2164, 2050, 1981)	C=O	Carboxylate ions	(Krumins et al., 2012)
BPC1 BPC2 BPC3 BPC4	1736	C=O stretching	Carboxylic acids, carbonyl group	(Cocozza et al., 2003; Krumins et al., 2012)
BPC1 BPC2 BPC3 BPC4	1720	C=O stretching of COOH/COOR	Acids, aldehydes, ketones, aromatic esters	(Cocozza et al., 2003; Gondar et al., 2005; Niemeyer et al., 1992)
BPC1 BPC2 BPC3 BPC4	1705	C=O stretch of COOH	Free organic acids, carboxylic acids	(Gondar et al., 2005)
BPC1 BPC2 BPC4	1608	C=C stretching and/or asymmetric C-O stretch in COO-	Lignin and other aromatics, or aromatic or aliphatic carboxylates	(Cocozza et al., 2003; Niemeyer et al., 1992)
BPC1 BPC2 BPC4	1512	C=C stretching	Lignin/phenolic backbone (e.g. benzene, pyridine)	(Cocozza et al., 2003)
BPC1 BPC2 BPC4	1466, 1373	C-H deformations	Phenolic (lignin) and aliphatic structures or methyl group	(Ning, 2011; Parker, 1971)
BPC1 BPC2 BPC4	1421	Symmetric C-O stretch from COO- or stretch and OH deformation from COOH	Carboxylate/carboxylic structures (humic acids)	(Parker, 1971)
APC2	1510-1412	Asymmetric stretch of CO ₃ ²⁻	Carbonates (calcite, dolomite)	(Müller et al., 2014)
BPC1 BPC2 BPC4	1267, 1228	C-O stretch of phenolic OH and/or arylmethylethers	Lignin	(Ibarra et al., 1996; Niemeyer et al., 1992)
BPC1 BPC2 BPC4	1201	C-O stretch	Esters, ethers, phenols	(Krumins et al., 2012)
APC1	1203-1078	Si-O asymmetrical stretching	Silicates (quartz, albite, orthoclase)	(Müller et al., 2014; Saikia et al., 2008)

BPC1 BPC2 BPC4	1157	C-OH stretch	Aliphatic OH	(Niemeyer et al., 1992)
APC2 APC4	1032-958	Si (Al)-O stretch	Silicates, mainly plagioclase and K-feldspar	(Müller et al., 2014)
BPC1 BPC2 BPC3	1059, 1032	Combination of C-O stretching and O-H deformation	Polysaccharides, alcoholic compounds	(Grube et al., 2006; Krumins et al., 2012)
APC1	876	Out-of-plane bending vibration of CO ₃ ²⁻	Carbonates (calcite, dolomite)	(Müller et al., 2014)
BPC2 BPC3 BPC4	895	Last H in 5-substituted benzene ring	Benzene ring	(Ning, 2011)
BPC1 BPC2	839	Aromatic CH out-of-phase bending	Lignin	(Niemeyer et al., 1992; Zaccheo et al., 2002)
APC1 APC2 APC3	798, 779	Si-O symmetrical stretching	Quartz	(Saikia et al., 2008)
BPC1 BPC2 BPC3	719	CH ₂ wag / in-phase rock	Long chain (>4 CH ₂) alkanes, methylene	(Larkin, 2011; Ning, 2011)
APC2 APC3	714	Si-O symmetrical bending	Silicates (quartz, albite, orthoclase)	(Saikia et al., 2008)
APC1 APC4	677-563	O-Si (Al)-O bending	Silicates, mainly plagioclase and K-feldspar	(Müller et al., 2014)
BPC1 BPC4	667	Vibrations of metal-O-metal, SO bending or PO vibrations	Metal oxides (eg. TiO ₂), sulphate, phosphate or silicates	(Colthup et al., 1990)
BPC1 BPC3 BPC4	559, 526	Vibrations of metal-O-metal, SO bending or PO vibrations	Metal oxides (eg. TiO ₂), sulphate, phosphate or silicates	(Colthup et al., 1990)
APC2 APC4	513	Si-O asymmetrical bending	Quartz, clays	(Saikia et al., 2008)
APC1	451-420	Si-O asymmetrical bending	Quartz, clays	(Saikia et al., 2008)